# Acute manipulation and real-time visualization of membrane trafficking and exocytosis in *Drosophila*

Jade Glashauser[1,§], Carolina Camelo[1,§], Manuel Hollmann[1], Wilko Backer[1], Thea Jacobs[1], Jone Isasti Sanchez[1], Raphael Schleutker[1], Dominique Förster[2], Nicola Berns[3], Veit Riechmann[3], and Stefan Luschnig[1,*]

[1]: Institute of Integrative Cell Biology and Physiology, Faculty of Biology and Cells in Motion (CiM) Interfaculty Center, University of Münster, D-48149 Münster, Germany

[2]: Present address: Department of Neurology, Faculty of Medicine and University Hospital Cologne, University of Cologne, D-50923 Cologne, Germany

[3]: Department of Cell and Molecular Biology, Medical Faculty Mannheim, Heidelberg University, D-68167 Mannheim, Germany

[§]: co-first authors

[*]**Correspondence:** luschnig@uni-muenster.de

**Running title:** Synchronized membrane trafficking *in vivo*

**Keywords:** Membrane trafficking, exocytosis, secretion, endoplasmic reticulum, Golgi apparatus, epithelium, tracheal system, tricellular junction, *Drosophila*

**Abstract**

Intracellular trafficking of secretory proteins plays key roles in animal development and physiology, but tools for investigating dynamics of membrane trafficking have been limited to cultured cells. Here we present a system that enables acute manipulation and real-time visualization of membrane trafficking through reversible retention of proteins in the endoplasmic reticulum (ER) in living multicellular organisms. By adapting the “retention using selective hooks” (RUSH) approach to *Drosophila*, we show that trafficking of GPI-linked, secreted, and transmembrane proteins can be controlled with high temporal precision in intact animals and cultured organs. We demonstrate the potential of this approach by analyzing the kinetics of ER exit and apical secretion and the spatiotemporal dynamics of tricellular junction assembly in epithelia of living embryos. Furthermore, we show that controllable ER-retention enables tissue-specific depletion of secretory protein function. The system is broadly applicable to visualize and manipulate membrane trafficking in diverse cell types *in vivo*.

## Introduction

Secreted and membrane proteins comprise substantial portions of metazoan proteomes (Meinken et al., 2015; Pei et al., 2018). The secretory apparatus ensures the correct delivery of these proteins to the extracellular space, the cell surface or intracellular membrane compartments, where they carry out a wealth of functions in cell adhesion, cell shape regulation, motility, and signaling during development and homeostasis. Accordingly, mutations in many secretory pathway components cause developmental defects and diseases (Schotman and Rabouille, 2009; Yarwood et al., 2020). While many insights into the organization and function of the secretory pathway were obtained in cultured mammalian cells and in yeast, analogous studies in intact multicellular organisms have been limited by the lack of adequate tools to manipulate membrane trafficking *in vivo*. Analyzing the dynamics of these processes is challenging, because different pools of a given protein species move simultaneously along multiple intracellular routes (synthesis, exocytosis, endocytosis, recycling, degradation) and localize in different membrane compartments, which cannot be separated at steady state. Therefore, the synthesis or transport of selected proteins needs to be synchronized to follow their routes through the secretory apparatus. Classical methods for synchronizing secretory protein trafficking either rely on temperature blocks (Griffiths et al., 1985) or drugs (e.g., Brefeldin A; Lippincott-Schwartz et al., 1989) to reversibly arrest intracellular transport, or employ special conditionally mis-folded or aggregated proteins that are retained in the endoplasmic reticulum (ER). Release of these proteins from the ER is achieved by shifting cells to permissive temperature (Kreis and Lodish, 1986; Lafay, 1974), by adding a small-molecule ligand (Casler et al., 2020; Rollins et al., 2000), or by illumination with UV light (Chen et al., 2013). Although these approaches have revealed fundamental insights into the organization and dynamics of the secretory apparatus, they are limited to special proteins (*e.g.*, the conditional thermosensitive mutant viral glycoprotein VSVGtsO45; Kreis and Lodish, 1986; Presley et al., 1997; Scales et al., 1997) and require treatments using non-physiological temperatures, drugs, or potentially damaging doses of UV light.

A powerful experimental system that avoids these limitations is the '*retention using selective hooks'* (RUSH) system (Boncompain et al., 2012). RUSH enables synchronization of trafficking by using a two component-system comprising (i) a secretory cargo protein fused with a fluorophore and a streptavidin-binding peptide (SBP) tag and (ii) a streptavidin (SA) "hook" protein targeted to a membrane "donor" compartment of choice by a signal sequence (*e.g.*, a KDEL motif for retention in the ER). SBP-Cargo and SA-hook proteins form a complex that is retained in the donor compartment (Fig. 1A). Addition of biotin rapidly dissociates the cargo-hook complex, triggering release of cargo from the donor compartment, and allows to follow the synchronized passage of the fluorescent cargo molecules through the secretory

apparatus. Importantly, RUSH is applicable to diverse cargo proteins, and their trafficking can be controlled at physiological temperatures using a non-toxic cell-permeable small molecule. This approach revealed important insights into the molecular events underlying ER exit (Shomron et al., 2021), ER-to-Golgi transport (Weigel et al., 2021; Westrate et al., 2020), intra-Golgi trafficking, and transport of cargo between the Golgi apparatus and the plasma membrane (Fourriere et al., 2016; Stalder and Gershlick, 2020). However, applications of the RUSH system have thus far been limited to cultured cells, which typically do not represent the complexity of tissues in multicellular organisms, where membrane trafficking is developmentally or physiologically regulated.

We present a set of tools that enable synchronization and visualization of membrane trafficking in intact animals and in cultured organs through reversible ER-retention of secretory proteins. The system is broadly applicable to investigate the spatiotemporal dynamics of secretory trafficking during development *in vivo*. Additionally, hook-induced ER retention provides a powerful approach to deplete membrane protein function in a tissue-specific manner.

## Design

### A two-component system for synchronization of membrane trafficking *in vivo*

To control trafficking of secretory proteins in *Drosophila*, we generated a set of cargo and hook proteins (Fig. 1B, Table S1) that can be expressed in a tissue-specific manner using the Gal4/UAS system (Brand and Perrimon, 1993). As a model cargo protein we chose the chitin deacetylase Serpentine (Serp), which is secreted by embryonic tracheal cells into the tube lumen (Luschnig et al., 2006; Wang et al., 2006). The N-terminal portion of Serp comprising the signal peptide and chitin-binding domain (CBD) is sufficient to direct apical secretion of a Serp(CBD)-GFP fusion protein, resembling the trafficking of full-length Serp-GFP protein, but unlike full-length Serp-GFP, expression of Serp(CBD)-GFP does not cause tracheal defects (Luschnig et al., 2006; Wang et al., 2006). Therefore, to generate model cargo proteins for RUSH experiments, we fused the N-terminal portion of Serp to Streptavidin-binding peptide (SBP, 38 aa; Keefe et al., 2001) followed by either the EGFP or mRFP coding sequence, resulting in Serp(CBD)-SBP-GFP (Serp-SBG) and Serp(CBD)-SBP-mRFP (Serp-SBR), respectively (Fig. 1B). When expressed in tracheal cells under the control of *btl*-Gal4, Serp-SBG and Serp-SBR accumulated in the tracheal lumen (Fig. 1C,D), resembling endogenous Serp protein (Luschnig et al., 2006; Wang et al., 2006). To retain the cargo proteins in the ER, we generated ER-resident hook constructs comprising either core streptavidin (SA) or the SA variant Streptactin (ST; Voss and Skerra, 1997) fused to the N-terminal signal peptide of Serp and a C-terminal ER retention signal (KDEL; Fig. 1B). When expressed in tracheal cells, SA-

KDEL and ST-KDEL were distributed in a perinuclear pattern (Fig. 1E,F) and co-localized with anti-KDEL immunostaining (Fig. 1G), indicating localization in the ER.

## Results

### SBP-tagged proteins can be retained in the ER by Streptavidin hooks

To test whether streptavidin hooks can retain Serp-SBG in the ER, we co-expressed SA-KDEL and Serp-SBG in embryonic tracheal cells. However, expression of a single-copy UAS-SA-KDEL transgene did not modify the distribution of Serp-SBG, which was secreted into the tracheal lumen like in control embryos not expressing SA-KDEL (Fig. 2A,B). Since SA forms a tetramer with two SBP binding sites (Barrette-Ng et al., 2013), we reasoned that an excess of SA-KDEL is required for efficient retention of Serp-SBG. Therefore, to increase SA-KDEL levels, we used a vector (pUAST∆SV40; Nelson et al., 2018) that yields approximately 5-fold higher expression levels compared to the pUAST vector (Brand and Perrimon, 1993) used for the first generation of SA-KDEL constructs. Indeed, combining one copy of UAST∆SV40-SA-KDEL (referred to as UAS-SA-KDEL(strong)) with one copy of UAS-Serp-SBG led to partial intracellular accumulation of Serp-SBG (Fig. 2C). To improve retention efficiency, we combined multiple copies of UAS-SA-KDEL(strong) transgenes with a single copy of UAS-Serp-SBG (Fig. 2C-E). The ratio of intracellular to luminal Serp-SBG signals increased with the dosage of SA-KDEL hooks, and maximal retention (median ratio of 1.2; n=15) was observed in 95% of embryos (n=40) expressing four copies of SA-KDEL(strong) (Fig. 2E,F). We generated strains carrying two insertions of UAS-SA-KDEL(strong) or UAS-ST-KDEL(strong), respectively, for each chromosome, enabling straightforward and versatile use in genetic crosses (Table S1; STAR Methods).

To ask whether hook-mediated ER retention works in different tissues and developmental stages, we generated flies expressing Serp-SBG ubiquitously under the control of the *ubiquitin* promoter (*ubi*-Serp-SBG) and used tissue-specific Gal4 drivers to express SA-KDEL or ST-KDEL hooks in selected tissues. In wing imaginal discs of third-instar larvae, Serp-SBG was secreted into the disc lumen (Fig. 2G). Expression of SA-KDEL or ST-KDEL hooks in the posterior compartment using *engrailed*-Gal4 (*en*-Gal4) led to intracellular retention of Serp-SBG in the hook-expressing cells (Fig. 2H). Likewise, Serp-SBG was retained in hook-expressing posterior compartment cells in the larval epidermis (Fig. 2I). Intracellular retention of Serp-SBG was also observed in adult tissues, such as ovarian follicle cells expressing the ER hooks (Fig. 2J,K). Thus, SA-KDEL and ST-KDEL hooks mediate efficient ER retention of an SBP-tagged secreted protein in different tissues throughout development.

119 We wondered whether elevated secretory cargo load caused by long-lasting expression of
120 streptavidin hooks or by hook-mediated ER-retention of secreted proteins might induce ER
121 stress and consequently activate the unfolded protein response (UPR; Hetz et al., 2020; Ryoo,
122 2015). To test for UPR induction, we used an Xbp1-GFP reporter construct, which yields a
123 nuclear-localized Xbp1-GFP fusion protein only after unconventional splicing of Xbp1-GFP
124 mRNA mediated by the nuclease IRE-1 in response to ER stress (Ryoo et al., 2007). Driving
125 Xbp1-GFP expression in tracheal cells of control embryos did not result in nuclear Xbp1-GFP
126 signals (Fig. S1A,K), whereas nuclear Xbp1-GFP was induced upon RNAi-mediated
127 knockdown of the ER chaperone Heat shock protein 70 cognate 3 (Hsc70-3; Fig. S1E,K),
128 which is required for protein folding and quality control in the ER (Chow et al., 2015). Nuclear
129 Xbp1-GFP signals were not detectable in tracheal cells expressing two copies of SA-KDEL
130 (Fig. S1B,K), but appeared in a subset of cells expressing four copies of SA-KDEL (Fig.
131 S1C,K), suggesting that SA-KDEL can induce ER stress in a dosage-dependent manner.
132 However, this was not associated with morphological abnormalities or cell death. Xbp1-GFP
133 levels did not increase when Serp-SBR was retained by SA-KDEL in the ER of tracheal cells
134 (Fig. S1D,K), suggesting that ER retention of SBP-tagged cargo does not induce ER stress.
135 In ovarian follicle cells, nuclear Xbp1-GFP was not detectable in the presence of either two or
136 four copies of SA-KDEL, and only rare nuclei showed Xbp1-GFP signals when Serp-SBR was
137 retained in the ER (Fig. S1F-I, L), whereas treatment with the reducing agent Dithiothreitol
138 (DTT) led to Xbp1-GFP accumulation throughout the follicle epithelium (Fig. S1J,L). Thus,
139 while high levels of SA-KDEL expression can induce ER stress in tracheal cells, ER stress
140 was not induced in follicle cells, consistent with the notion that the sensitivity to ER cargo load
141 differs between cell types (Sone et al., 2013).

142 **Injection of biotin triggers ER exit and secretion of SBP-tagged cargo**

143 To test whether SA-KDEL-mediated ER retention is reversible, we injected biotin (1 mM) into
144 the hemocoel of embryos (stage 15) expressing Serp-SBG (one copy) and SA-KDEL (four
145 copies) in tracheal cells (Fig. 3). We analyzed the distribution of Serp-SBG in the multicellular
146 dorsal trunk (DT; Fig. 3A,B, Movie S1, Movie S2) and in unicellular dorsal branches (Fig. 3C,
147 Movie S3). Before biotin injection, Serp-SBG was distributed in a perinuclear pattern in
148 tracheal cells. Approximately two minutes after biotin injection, Serp-SBG started to
149 accumulate in discrete intracellular puncta. Six to ten minutes after injection, Serp-SBG signals
150 in the tracheal lumen started to increase rapidly, while intracellular signals concomitantly
151 decreased (Fig. 3A,C,D, Movie S1), indicating that Serp-SBG passed the secretory pathway
152 and started to be secreted as early as six minutes after release from the ER. Luminal Serp-
153 SBG signals were maximal after 30 minutes and then declined gradually, while intracellular
154 signals concurrently leveled off (Fig. 3D), suggesting that the supply of ER-retained Serp-SBG

155 protein was depleted. The kinetics of ER release and luminal secretion of Serp-SBG were
156 dependent on the concentration of injected biotin. 1 mM biotin induced rapid ER release,
157 whereas 10 µM biotin was not sufficient to induce release (n=3; Fig. S2, Movie S4). A slow
158 and steady increase in luminal Serp-SBG signals upon injection of 10 µM biotin, but no
159 concomitant reduction of intracellular signals, suggests that constant slow leakage of Serp-
160 SBG from the ER is compensated by newly synthesized Serp-SBG protein (Fig. S2).

161 From approximately 20 minutes after injection, Serp-SBG appeared in small intracellular
162 puncta (0.67 ± 0.12 µm diameter, mean ± s.d., n=15 puncta), which moved rapidly (0.43 ±
163 0.18 µm/s; mean ± s.d., n=22 puncta) and co-localized partially with Rab4-mRFP-positive
164 recycling endosomes (Fig. 3B,C', Movie S2, Movie S3). This suggests that secreted Serp-
165 SBG was internalized from the lumen and entered the endocytic pathway, consistent with
166 intense endocytic activity of tracheal cells during luminal clearance (Dong et al., 2013;
167 Tsarouhas et al., 2007). Taken together, these findings show that biotin injection triggers rapid
168 release of retained proteins from the ER, enabling synchronization and visualization of
169 secretory protein trafficking in living embryos.

170 **Serp-SBG rapidly passes the secretory apparatus**

171 We used this system to analyze the dynamics of Serp-SBG transport through the early
172 secretory apparatus. Embryonic tracheal cells contain on the order of a dozen dispersed Golgi
173 stacks (Armbruster and Luschnig, 2012; Förster et al., 2010), each of which resides adjacent
174 to a transitional ER (tER; Schweizer et al., 1990) unit, where secretory cargo proteins are
175 collected at clusters of ER exit sites (ERES; Bannykh et al., 1996) before leaving the ER. We
176 labeled ERES using an mCherry-tagged version of the COPII component Sec24AB (mCherry-
177 Sec24; Fig. 4, Fig. S3), which colocalized with the ERES marker Sec16 (Fig. S3A; Ivan et al.,
178 2008) and localized adjacent to the *cis*-Golgi marker GRASP65-GFP (Fig. S3B; Yang et al.,
179 2021).

180 To analyze the transit of Serp-SBG through the ER-Golgi interface, we measured Serp-SBG
181 signals within spherical volumes, each of which enclosed an mCherry-Sec24-labelled ERES
182 (Fig. 4A,B; Movie S5). Shortly after biotin injection, Serp-SBG rapidly accumulated at
183 mCherry-Sec24-labelled ERES in a synchronous fashion with a peak at seven minutes after
184 injection, and subsequently decreased over 30 minutes (Fig. 4B; n=996 mCherry-Sec24 units
185 in 7 embryos). Afterwards, Serp-SBG levels at ERES leveled off, suggesting that most of the
186 retained Serp-SBG protein has exited the ER. Comparable profiles of Serp-SBG levels were
187 detected in all mCherry-Sec24-labelled tER units analyzed, independent of their position along
188 the apical-basal axis of tracheal cells (Fig. 4C), suggesting that Serp-SBG passes through all
189 ERES/Golgi units in a uniform fashion.

190 High-resolution imaging of individual ERES/Golgi units revealed that Serp-SBG started to
191 accumulate at ERES, as detected by colocalization with mCherry-Sec24, approximately two
192 minutes after biotin injection (Fig. 4D,E; Movie S6). Shortly after, the bulk of Serp-SBG shifted
193 into clusters adjacent to and partially overlapping with the mCherry-Sec24-labelled ERES,
194 before disappearing approximately 20 minutes after biotin injection (Fig. 4D, Movie S6). The
195 area of overlap between mCherry-Sec24 and Serp-SBG signals was maximal between two
196 and six minutes and then dropped to zero approximately 12 minutes after biotin injection (Fig.
197 4E). These findings suggest that after residing in the tER or at ERES for approximately four
198 minutes, the bulk of Serp-SBG translocates to an adjacent compartment, corresponding to
199 Golgi cisternae (Yang et al., 2021), where the protein spends approximately eight minutes
200 before exiting the Golgi apparatus (Fig. 4E). Thus, RUSH allows analyzing the dynamics of
201 trafficking between different membrane compartments *in vivo*.

202 **RUSH enables control over trafficking of endogenous proteins**

203 Having shown that secretion of Serp-SBG can be controlled using SA hooks, we asked
204 whether the system is also applicable to endogenous proteins. To this aim, we took advantage
205 of the Cambridge protein trap insertion (CPTI; Lowe et al., 2014; Lye et al., 2014) fly strains,
206 in which a given protein is tagged with Venus-YFP and two flanking StrepII tags (StrepII-
207 Venus-YFP-StrepII; SVS) encoded by an artificial exon inserted into the endogenous gene
208 locus (Fig. 5, Fig. S4). We tested transmembrane (Basigin (Bsg), Echinoid (Ed), Gliotactin
209 (Gli), Neurexin 4 (Nrx4), Notch (N), Sidekick (Sdk)), Glycosylphosphatidylinositol (GPI)-
210 anchored (Fasciclin 2 (Fas2), Lachesin (Lac)), and secreted (Chitin deacetylase-like 4; Cda4)
211 proteins carrying an SVS tag in their extracellular portion (Fig. S4). To test whether localization
212 of these proteins can be manipulated using ER hooks, we drove expression of ER hooks in
213 epidermal stripes (using *en*-Gal4 or *hh*-Gal4) in heterozygous animals carrying one copy of
214 the SVS-tagged locus (Fig. 5, Fig. S4). To maximize the affinity for StrepII-tagged proteins,
215 we used Streptactin (ST)-KDEL instead of SA-KDEL hook proteins, since the StrepII tag binds
216 with higher affinity to Streptactin (ST-StrepII: $K_d = 10^{-6}$ M; Voss and Skerra, 1997) than to
217 streptavidin (SA-StrepII: $K_d = 72 \times 10^{-6}$ M; Kim et al., 2010). Expression of two copies of ST-
218 KDEL indeed led to ER retention of SVS-tagged proteins, as shown for Fas2::SVS in the
219 embryonic and larval epidermis, larval imaginal discs, and in adult ovarian follicle cells (Fig.
220 5A-F). While efficient ER retention was observed for the majority of SVS-tagged proteins
221 tested (Cda4, Fas2, Gli, Notch, Nrx4; Fig. S4), some proteins showed partial (Lac; Fig. S4H)
222 or no detectable retention (Bsg, Ed, Sdk; Fig. S4D-F), suggesting that cargo protein
223 abundance or accessibility of the SVS tag can influence the efficiency of ST-KDEL-induced
224 ER retention.

225 In all cases tested, biotin injection triggered rapid release of the retained proteins from the ER.
226 For instance, the SJ protein Nrx4::SVS was retained in the ER in ST-KDEL-expressing
227 epidermal cells, while it was localized at lateral membranes in adjacent control cells (Fig. S4K).
228 Within four minutes after biotin injection, Nrx4::SVS accumulated in puncta resembling
229 ERES/Golgi clusters. After fifteen minutes, Nrx4::SVS became detectable at lateral plasma
230 membranes (Fig. S4K), suggesting that the newly released Nrx4::SVS protein was
231 incorporated into SJs. Taken together, these findings show that RUSH enables control over
232 ER exit and trafficking of exogenous as well as endogenous transmembrane, GPI-anchored,
233 and secreted proteins in embryos.

234 **Control of membrane trafficking in organs cultured *ex vivo***

235 We next tested whether the system can be used also to control secretory trafficking in organs
236 cultured *ex vivo*. To this aim, we cultivated ovarian follicles of females expressing endogenous
237 Fas2::SVS (CPTI 000483; Lye et al., 2014). The NCAM homolog *Fas2* encodes
238 transmembrane and GPI-anchored isoforms (Neuert et al., 2020), all of which carry the SVS
239 tag in the Fas2 ectodomain (Figure 5A). Fas2::SVS localizes at lateral membranes of follicle
240 cells in pre-vitellogenic egg chambers (Fig. 5E). Expression of ST-KDEL in the follicle
241 epithelium of heterozygous *Fas2::SVS/+* females led to retention of Fas2::SVS in the
242 perinuclear ER (Fig. 5F, Fig. S5). Addition of biotin (1.5 mM final concentration) to the culture
243 medium triggered release of Fas2::SVS from the ER after approximately two minutes (n=8;
244 Movie S8). At the same time, Fas2::SVS began to accumulate in large puncta resembling ER
245 exit sites, and became detectable at lateral cell membranes from approximately 20 minutes
246 after biotin addition (Fig. 5G, Movie S8).

247 **Characterizing the secretory route of Fasciclin2 protein**

248 To visualize intermediate steps of Fas2::SVS trafficking to the plasma membrane, we fixed
249 follicles at different time points after biotin-induced ER-release and labeled specific
250 compartments of the secretory pathway by immunostaining (Fig. S5A-G). In stage 6 follicles,
251 Fas2::SVS was retained in RFP-KDEL-positive perinuclear ER and in ER structures that were
252 enriched in the basal cytoplasm (Fig. S5A). Within ten minutes after biotin addition, Fas2::SVS
253 redistributed to large puncta (0.349 ± 0.1 µm diameter, mean ± s.d.; n=1827 puncta in 286
254 cells) that localized adjacent to RFP-KDEL-positive ER structures and were labeled by the
255 trans-Golgi marker Golgin245 (Fig. S5B,D), indicating that Fas2::SVS has passed the ER and
256 reached the trans-Golgi network. After 30 minutes, Fas2::SVS appeared in numerous smaller
257 puncta (0.052 ± 0.02 µm diameter, mean ± s.d.; n=786 puncta in 139 cells), which did not
258 overlap with the late-endosomal marker Rab7 (Fig. S5C,E). These Fas2::SVS-positive puncta
259 were distributed along parallel F-actin bundles underneath the basal plasma membrane (Fig.

260 S5G), suggesting that Fas2::SVS-carrying vesicles are transported along basal actin
261 filaments. Indeed, live imaging of follicles 30 minutes after ER release revealed that Fas2::SVS
262 vesicles moved directionally towards the lateral plasma membrane (Fig. S5H,I). The vesicles
263 travelled in parallel to the orientation of the basal F-actin bundles at a speed (0,29 ± 0,1
264 µm/sec, n=10 vesicles) that is consistent with myosin-based transport (Mehta et al., 1999).
265 Thus, RUSH-based analysis suggests that Fas2 protein is transported through basal ER and
266 Golgi compartments to dynamic vesicles that move, presumably along basal actin filaments,
267 to the plasma membrane. These results demonstrate that RUSH allows to characterize the
268 route of a secretory protein from the ER through the Golgi apparatus to late steps, including
269 transport in secretory vesicles.

270 **Real-time analysis of tricellular junction assembly**

271 Building on these results, we employed RUSH to investigate the assembly of tricellular
272 junctions (TCJs) in embryonic epithelia. The transmembrane proteins Anakonda (Aka),
273 Gliotactin (Gli) and M6 accumulate at epithelial cell vertices, where they organize TCJs
274 essential for epithelial barrier function, but how TCJ proteins are targeted to vertices is not
275 clear. Analyzing the spatiotemporal dynamics of TCJ assembly has not been possible thus
276 far, because recruitment of TCJ proteins to cell vertices cannot be visualized under steady-
277 state conditions. We therefore used RUSH to synchronize trafficking of the TCJ protein Gli in
278 the embryonic epidermis. Flies carrying the homozygous viable *Gli*$^{CPTI002805}$ allele (Lye et al.,
279 2014) produce functional Gli::SVS protein that localizes to TCJs like wild-type Gli protein (Fig.
280 6A; Wittek et al., 2020). Expression of ST-KDEL in epidermal stripes of heterozygous
281 *Gli*$^{CPTI002805}$ embryos led to ER retention of Gli::SVS, while Gli::SVS localized to TCJs in
282 adjacent control cells (Fig. 6A,B). The uniform Gli::SVS signal in the ER of ST-KDEL-
283 expressing cells decreased shortly after biotin injection, and after 2 minutes Gli::SVS
284 accumulated at puncta resembling ERES-Golgi clusters (Fig. 6B,C, Movie S7). Approximately
285 10 minutes after biotin injection, Gli::SVS signals began to increase sharply at TCJs and to a
286 lesser degree at bicellular junctions (BCJs). Signals at BCJs no longer increased after 15
287 minutes, while signals at TCJs continued to increase (Fig. 6B,C). Of note, Gli::SVS signal was
288 still visible at BJCs of ST-KDEL-expressing cells 30 minutes after release, whereas Gli::SVS
289 was not visible at BCJs of control cells (Fig. 6B, 30 min). Together, these findings suggest that
290 a fraction of Gli::SVS protein is initially delivered to BCJs and subsequently redistributed to
291 TCJs. Interestingly, the newly released Gli::SVS protein was not incorporated along the entire
292 length of the vertices but accumulated in a single spot at the apical side of each TCJ (Fig.
293 6D,E, Movie S7). This suggests that growing TCJs are extended in a polarized fashion by
294 addition of new material to the apical side of the junctional complex, resembling the behavior
295 of growing bicellular SJs (Babatz et al., 2018). These findings demonstrate how

296 synchronization of membrane trafficking can be employed to gain insights into the
297 spatiotemporal dynamics of junctional assembly in developing tissues *in vivo*.

298 **Hook-induced ER retention enables tissue-specific interference with protein secretion**

299 Finally, we asked whether hook-induced ER retention could be employed to interfere with
300 secretory protein function. To this aim, we analyzed the effect of ER retention of the Notch (N)
301 receptor on cell fate specification. In the embryonic tracheal system, the N ligand Delta (Dl) is
302 expressed at elevated levels in tracheal fusion cells (FCs) at branch tips and activates N
303 signaling in adjacent stalk cells to prevent these cells from adopting tip cell fate (Fig. 7A).
304 Accordingly, *N* mutations cause excessive FC specification (Ikeya and Hayashi, 1999;
305 Llimargas, 1999; Steneberg et al., 1999). To test whether ST-KDEL-induced ER retention of
306 N protein in tracheal cells can reproduce the tracheal phenotype of *N* mutations, we used the
307 $N^{SVS\text{-}CPTI002347}$ allele (referred to as *N::SVS*), which produces N::SVS protein with an SVS tag
308 inserted into the N ectodomain (Lye et al., 2014). N::SVS protein was weakly detectable in
309 embryonic tracheal (Fig. 7B) and larval wing imaginal disc cells (Fig. 7D). Homozygous
310 (female) and hemizygous (male) *N::SVS* flies were phenotypically normal and fertile,
311 indicating that N::SVS protein is functional. The majority of embryos carrying *N::SVS* showed
312 normal tracheal cell specification with a pair of FCs (discernible by expression of the
313 transcription factor Dysfusion (Dysf)) at each tracheal metamere boundary (Fig. 7B), while
314 supernumerary FCs were found in 12% (n=17) of *N::SVS/*+ heterozygous and in 43% (n=14)
315 of *N::SVS/Y* hemizygous embryos (at least one extra FC per embryo; Fig. S6A,B,G).
316 Expression of two copies of ST-KDEL in tracheal cells of *N::SVS* embryos led to intracellular
317 accumulation of N::SVS protein (Fig. 7C) and to excessive specification of FCs in 31% (n=13)
318 of *N::SVS/*+ heterozygous and in 76% (n=21) of *N::SVS/Y* hemizygous embryos (Fig.
319 S6C,D,G). Increasing the dosage of *btl*-Gal4 from one to two copies led to fully penetrant
320 (100%; n=11) ectopic FC specification in *N::SVS/Y* hemizygous embryos (Fig. S6F,G)
321 resembling the tracheal defects in N mutants (Ikeya and Hayashi, 1999; Llimargas, 1999;
322 Steneberg et al., 1999), indicating that hook-induced ER retention of N protein effectively
323 blocks N signaling. Moreover, ST-KDEL expression under the control of *en*-Gal4 led to ER
324 retention of N::SVS protein in the posterior compartment of wing imaginal discs in third-instar
325 larvae (Fig. 7D). Adult flies showed characteristic wing margin defects and thickened wing
326 veins, resembling the wing defects of $N^{1}$ mutants, but restricted to the posterior wing
327 compartment (Fig. 7E-G). Together, these findings demonstrate that hook-induced ER
328 retention can be used to deplete the functional pool of a membrane protein by interfering with
329 its secretion in a tissue-specific manner.

330

331 ## Discussion

332 We present a system that enables visualizing the dynamics of membrane trafficking through
333 reversible retention of proteins in the secretory apparatus in a multicellular organism. We show
334 that secreted, transmembrane, and GPI-linked proteins are efficiently retained in the ER by
335 streptavidin hook proteins in *Drosophila* embryos, larvae, and adults. Hook-mediated ER
336 retention is rapidly reversed upon addition of biotin, allowing to synchronize intracellular
337 trafficking and to release fluorescent-marked cargo proteins with high temporal precision in a
338 burst of secretion. The system enables control of exogenous and endogenous proteins, is
339 readily combined with available endogenously tagged protein-trap alleles, and is applicable to
340 various tissues in intact animals, as well to organs cultured *ex vivo*. We demonstrate the utility
341 of this approach for analyzing the kinetics of ER-Golgi-trafficking and protein secretion, and
342 the spatiotemporal dynamics of tricellular junction assembly in embryonic epithelia. Finally, we
343 show that hook-induced ER retention can be employed to deplete the functional pool of
344 proteins, allowing to generate tissue-specific loss-of-function conditions.

345 While methods for synchronizing secretory trafficking have been used extensively in cultured
346 cells (Boncompain et al., 2012; Chen et al., 2013; Presley et al., 1997; Scales et al., 1997;
347 Weigel et al., 2021), adopting these systems to multicellular organisms has been challenging.
348 A first example of synchronized trafficking in *Drosophila* utilized a regulatable secretory protein
349 (ESCargo, Erv29/Surf4-dependent secretory cargo; Casler et al., 2020) to analyze the kinetics
350 of secretion in a multicellular tissue *ex vivo*. However, this system is based on reversible
351 aggregation of an engineered protein and cannot readily be applied to other cargoes. RUSH
352 represents a versatile two-component system based on short peptide tags (SBP or StrepII)
353 that can be fused to any protein of interest and enable control at physiological temperature by
354 biotin, an endogenous vitamin (Boncompain et al., 2012). Importantly, RUSH employs the
355 physiological KDEL-receptor-based protein retrieval mechanism to achieve ER retention of
356 secretory cargo. This mechanism of protein retention is active in all cells under physiological
357 conditions, and contrasts with other, more artificial experimental systems, which are based on
358 reversible protein aggregation (Casler et al., 2020; Chen et al., 2013; Rollins et al., 2000) or
359 misfolding (Kreis and Lodish, 1986), conditions known to induce the unfolded protein response
360 (Hetz et al., 2020). Secretory cargo is released by dissociating ER-retained streptavidin-cargo
361 complexes using a natural, non-toxic agent. Injection of biotin at concentrations exceeding
362 physiological levels did not cause evident toxicity in *Drosophila* embryos. However,
363 endogenous biotin may reduce the efficacy of hook-induced cargo retention by occupying SBP
364 binding sites on streptavidin. We show that this problem can be overcome by increasing the
365 dosage of streptavidin-KDEL hook proteins. Fly strains carrying multiple copies of streptavidin-

366 KDEL transgenes (Table S1) enable straightforward and versatile application of these tools in
367 genetic crosses.

368 The use of RUSH revealed rapid ER exit and passage of the Golgi apparatus by secretory
369 proteins in epithelia *in vivo*. While mammalian cells typically contain a single pile of
370 interconnected Golgi stacks with tubular ERES extending between ER and Golgi (Weigel et
371 al., 2021), *Drosophila* cells contain several dispersed Golgi mini-stacks (Kondylis and
372 Rabouille, 2009) adjacent to C- or ring-shaped ERES (Reynolds et al., 2019; Yang et al.,
373 2021). Despite these differences, ER-Golgi trafficking in *Drosophila* tracheal cells occurred on
374 similar time scales (2 to 3 min for Serp-SBG) as described for various GPI-linked and
375 transmembrane RUSH cargos in mammalian cells (Weigel et al., 2021). Overexpressed Serp-
376 SBG was released from the ER with similar kinetics as endogenous proteins (Fas2::SVS,
377 Gli::SVS; Nrx4::SVS), suggesting that rapid ER-Golgi traffic is not due to cargo
378 overexpression, which could in principle activate autoregulatory mechanisms that control
379 secretory flux in response to elevated cargo load (Subramanian et al., 2019). Unlike in
380 mammalian cells, where trafficking of TNF-alpha led to a two-fold size increase of ERES
381 (Weigel et al., 2021), we did not detect obvious changes in the size of mCherry-Sec24-labelled
382 ERES upon ER-release of cargo in tracheal cells. Previous work indicated that subsets of
383 Golgi units in *Drosophila* epithelial cells contain distinct sets of glycosylation enzymes,
384 suggesting possible functional differences between Golgi units (Yano et al., 2005). For the
385 secretory proteins tested here, we did not detect evident differences in the rate of cargo
386 passage between different ERES, all of which appeared to be traversed in an approximately
387 uniform fashion. This suggests that functional differences between individual ER-Golgi units
388 are not reflected by the dynamics of cargo passage through these units.

389 Our real-time analysis of tricellular junction assembly demonstrates the potential of the RUSH
390 assay for elucidating the intracellular routes of proteins and the kinetics of their assembly into
391 complex structures at the tissue level in living organisms. Importantly, the ability to synchronize
392 and follow the dynamics of these processes in real time reveals insights that are not apparent
393 at steady state or by endpoint analyses, as highlighted by our analysis of tricellular junction
394 assembly. In addition to visualizing secretory trafficking in intact living animals, we
395 demonstrate that hook-induced protein re-localization can be used to interfere with protein
396 function. Manipulating proteins rather than gene expression is required in situations where
397 protein perdurance due to slow turnover upon genetic knockout or RNAi-mediated knock-
398 down precludes loss-of-function phenotypes. While nanobody-based approaches allow to re-
399 localize (Harmansa et al., 2017), trap (Matsuda et al., 2021) or degrade proteins (Caussinus
400 et al., 2012), reversible retention by streptavidin hooks offers the additional potential to acutely
401 restore protein localization and function upon addition of biotin, enabling powerful functional

402 experiments with precise temporal control. For instance, releasing a signaling molecule from
403 a defined source at a defined time will allow to determine the signaling molecule´s mode of
404 dispersal in the tissue and the kinetics of cellular responses across a field of cells.

405 **Limitations**

406 While RUSH is in principle applicable to any secretory protein, the system requires a short
407 peptide tag (SBP: 38 aa; Keefe et al., 2001; StrepII: 10 aa; Voss and Skerra, 1997) to be
408 inserted into the luminal portion of the protein, without interfering with protein folding or
409 trafficking. We showed that this can be readily achieved for both exogenous and endogenous
410 proteins. Sampling a collection of StrepII-tagged protein trap lines (Lye et al., 2014) revealed
411 that 6 (67%) out of 9 tested proteins are efficiently retained in the ER by streptavidin-KDEL
412 hooks. Approximately 100 such protein trap insertions in membrane-associated or secreted
413 proteins are available (https://kyotofly.kit.jp/stocks/documents/CPTI.html) and provide a
414 valuable resource as potential cargo proteins for RUSH experiments. However, the StrepII tag
415 must be accessible in the luminal part of the protein for binding to streptavidin, and
416 inaccessibility of the StrepII tag may explain the lack of ER-retention observed with some of
417 the tested CPTI lines. Generating additional StrepII-tagged cargo lines is straightforward using
418 recombinase-mediated cassette exchange (RCME; Venken et al., 2011) or CRISPR-Cas9-
419 based genome editing approaches.

420 Long-term expression of streptavidin-KDEL may cause ER stress due to increased cargo load.
421 However, we found that streptavidin-KDEL expression and ER-retention of RUSH cargo
422 proteins did not generally induce ER stress, but that only high levels of ER hooks induced ER
423 stress in a cell-type-specific manner. Consistent with our findings, certain cell types (*e.g*.
424 secretory epithelia) show constitutive induction of XBP1-GFP reporters in the absence of
425 genetic or pharmacological stressors, suggesting that basal activity of the IRE1/XBP1 ER
426 stress sensing system is part of normal *Drosophila* development (Ryoo et al., 2007; Sone et
427 al., 2013). Elevated secretory load was not accompanied by cell death or developmental or
428 morphological abnormalities. However, prolonged streptavidin expression in certain tissues
429 may cause developmental delays due to depletion of biotin, an essential vitamin. This potential
430 problem can be circumvented by tuning the levels or timing of streptavidin expression, *e.g*.
431 using temperature-sensitive Gal80 to conditionally control Gal4 activity (McGuire et al., 2004).

432 While RUSH currently provides temporal control over membrane trafficking, combining the
433 system with orthogonal opto-chemical tools (*e.g*. photoactivatable “caged” biotin; Terai et al.,
434 2011) or with photoactivatable or photoconvertible proteins will enable precise spatial and
435 temporal manipulation of cellular processes. We anticipate that the application and further

436 development of the tools presented here will reveal new insights into the dynamics and
437 functions of secretory trafficking in various model organisms.

438

439 **Materials and methods**

440 **Fly husbandry and embryo collection**

441 Flies were reared on standard cornmeal-molasses-yeast food. The efficiency of streptavidin-
442 mediated ER retention was strongly dependent on the type of dietary yeast, presumably due
443 to differences in biotin content. Ovaries and embryos from flies that were fed fresh yeast
444 showed more efficient ER retention compared to flies that were fed yeast paste prepared from
445 dry yeast. For RUSH experiments, adult flies were therefore kept on apple juice agar plates
446 with yeast paste prepared from fresh baker´s yeast (Fala) for two days before collection of
447 embryos or ovaries. To reduce the availability of biotin, yeast paste was supplemented with
448 Avidin (50 ppm; Sigma A9275).

449 ***Drosophila* strains and genetics**

450 Unless noted otherwise, *Drosophila* stocks are described in FlyBase. Cambridge protein trap
451 insertion (CPTI) lines (Lowe et al., 2014; Lye et al., 2014) were obtained from the DGRC stock
452 center (Kyoto, Japan) for Basigin (Bsg; CPTI 100050), Chitin deacetylase-like 4 (Cda4; CPTI
453 002501), Echinoid (Ed; CPTI 000616), Fasciclin 2 (Fas2; CPTI 000483), Gliotactin (Gli; CPTI
454 002805), Lachesin (Lac; CPTI 002601), Neurexin 4 (Nrx4; CPTI 001977), Notch (N; CPTI
455 002347) and Sidekick (Sdk; CPTI001692). Other fly stocks were UAS-mCherry-Sec24 (this
456 work), UAS-Rab4-mRFP (Bloomington 8505), UAS-GRASP65-GFP (Bloomington 8507),
457 UASp-RFP-KDEL (Bloomington 30910), UAS-mCherry-NLS, UAS-CyPET-nls (Caussinus et
458 al., 2008), UAS-palm-mKate2 (Caviglia et al., 2016), UAS-palm-mNeonGreen (Sauerwald et
459 al., 2017), UAS-SerpCBD-GFP (Luschnig et al., 2006), UAS-Xbp1-GFP (Ryoo et al., 2007),
460 UAS-Hsc70-3 RNAi (Bloomington 80420), *ubi*-Dlg1::TagRFP (Pinheiro et al., 2017), *btl*-GAL4,
461 *en*-GAL4, *GR1*-Gal4, *hh*-GAL4, *CyO Dfd-GMR-nvYFP, TM6b Dfd-GMR-nvYFP* (Le et al.,
462 2006). *TM3 Ser Dfd-GMR-nvYFP* was generated by transposase-mediated mobilization of the
463 *P[Dfd-GMR-nvYFP]* P-element from the *FM7i Dfd-GMR-nvYFP* chromosome (Le et al., 2006)
464 onto a *TM3 Ser* chromosome.

465 **Transgenic constructs**

466 The following cargo and hook constructs were generated in this work: UAS-Serp-SBG
467 (pUAST-SerpCBD-SBP-GFP, pUASp-SerpCBD-SBP-GFP), *ubi*-Serp-SBG (pWRpUbiqPE-
468 SerpCBD-SBP-GFP), UAS-Serp-SBR (pUAST-Serp(CBD)-SBP-mRFP), UAS-streptavidin-

469 KDEL (pUAST-SA-KDEL, pUAST∆SV40-SA-KDEL), UAS-Streptactin-KDEL (pUAST∆SV40-
470 ST-KDEL).

471 Serp(CBD)-SBP-GFP (Serp-SBG) was generated as follows: A DNA fragment containing the
472 N-terminal portion of the Serp coding sequence including the signal peptide (aa1-25; Luschnig
473 et al., 2006) and chitin-binding domain (CBD), followed by one copy of streptavidin-binding
474 peptide (SBP; 38 aa; Keefe et al., 2001), was synthesized and cloned into pUC57-KanR
475 (GenScript Inc.). The insert was subcloned as an EcoRI-NotI fragment into pUASTattB-EGFP
476 to introduce a C-terminal EGFP tag. The construct was integrated into the attP-3B
477 (VK00037)/22A3 landing site using PhiC31-mediated site-specific integration (Bischof et al.,
478 2007). The Serp(CBD)-SBP-GFP fragment was also subcloned into pUASp to generate
479 pUASp-SerpCBD-SBP-GFP, which was transformed into *y w* flies via P-element mediated
480 transgenesis. For ubiquitous expression under the control of the *ubiquitin* promoter, the Serp-
481 SBG coding sequence was inserted into pWRpUbiqPE and transformed into *y w* flies via P-
482 element mediated transgenesis.

483 Serp(CBD)-SBP-mRFP (Serp-SBR) was generated as follows: A DNA fragment comprising
484 the N-terminal portion of the Serp coding sequence, an SBP tag and the mRFP coding
485 sequence was synthesized and cloned into pUC57-KanR (GenScript Inc.) and subcloned as
486 an EcoRI-XBaI fragment into pUASTattB (Bischof et al., 2007). The construct was integrated
487 into the attP40/25C6 landing site.

488 Streptavidin-KDEL (SA-KDEL) was generated by fusing the core SA coding sequence
489 (UniProt P22629; aa 36-163; reverse-translated using the *Drosophila melanogaster* codon
490 distribution) to the N-terminal signal peptide of Serp (aa 1-25) and to a C-terminal four-amino-
491 acid ER retention signal (KDEL). The SA-KDEL protein sequence was reverse-translated
492 using the *Drosophila melanogaster* codon usage distribution, synthesized, cloned into pUC57-
493 KanR (GenScript, Inc.), and subcloned as an EcoRI-XbaI fragment into pUASTattB (Bischof
494 et al., 2007) and pUAST∆SV40attB, respectively. pUAST∆SV40attB is a pUASTattB derivative
495 lacking the SV40 3'-UTR that targets transcripts for nonsense-mediated mRNA decay.
496 Deletion of the intron-containing 3'-UTR results in stabilized transcripts and approximately 5-
497 fold higher expression levels compared to pUAST transgenes (Nelson et al., 2018). The
498 pUAST∆SV40attB-SA-KDEL construct was integrated into the attP40/25C6, attPZH-51C1,
499 attP-3B(VK00031)/62E1 and attPZH-86Fa landing sites. The pUAST-SA-KDEL construct was
500 integrated into the attP2/68A4 landing site.

501 Streptactin-KDEL (ST-KDEL) was generated by fusing the ST coding sequence (Voss and
502 Skerra, 1997) to the N-terminal signal peptide of Serp (aa 1-25) and a C-terminal ER retention
503 signal (KDEL). This fragment was synthesized, inserted in pUC57-KanR (GenScript, Inc.), and

504 subcloned as an EcoRI-KpnI fragment in pUAST∆SV40attB. The construct was integrated into
505 the attPZH-2A, attP18/6C12, attP4/12C6 (X-chromosome), attP40/25C6, attPZH-51C1
506 (second chromosome), attP-3B(VK00031)/62E1 and attPZH-86Fa (third chromosome)
507 landing sites.

508 To increase the copy number of UAS-SA-KDEL or UAS-ST-KDEL transgenes, two insertions
509 on the X-chromosome (attPZH-2A, attP18/6C12), second chromosome (attP40/25C6, attPZH-
510 51C1), or third chromosome (attP-3B(VK00031)/62E1, attPZH-86Fa), respectively, were
511 recombined. A strain carrying four copies of UAS-SA-KDEL was generated by combining two
512 insertions on the second chromosome (attP40/25C6, attPZH-51C1) with two insertions on the
513 third chromosome (attP-3B(VK00031)/62E1, attPZH-86Fa).

514 mCherry-Sec24 was generated by amplifying the *Sec24AB* coding region (including introns)
515 from genomic DNA of Oregon R flies using oligonucleotides BamHI-sec24-F (5'-
516 ATATGGATCCATGTCGACTTACAATCCGAAC) and sec24-XbaI-R (5'-
517 TATATCTAGATCGCTTCGTGCTTCTAGTCA). The PCR product was cut with BamHI and
518 XbaI and the resulting fragment was inserted into pUASTattB-mCherry-mcs (BglII-XbaI) to
519 fuse mCherry to the N-terminus of Sec24. The pUASTattB-mCherry-Sec24 construct was
520 integrated into the attP/ZH-86Fa landing site. After establishing a homozygous viable
521 transformant line, the $w^+$ and *3xP3-RFP* markers of the attP/ZH-86Fa landing site were
522 removed using Cre-mediated recombination.

523 UAS-Fas2B-SVS (GPI-anchored Fas2 isoform B, carrying the SVS tag at the same position
524 as in the $Fas2^{CPTI000483}$ protein trap allele) was generated by isolating *Fas2* cDNAs from
525 $Fas2^{CPTI000483}$ homozygous females. Total RNA was extracted from ovaries using TRIzol
526 reagent (Thermo Fisher, 15596026). polyA+ mRNA was isolated using Dynabeads mRNA
527 purification kit (Thermo Fisher, 61006). First-strand cDNA was generated using ProtoScript
528 first strand cDNA synthesis kit (NEB, E6300S) with oligo-dT primers. cDNAs corresponding to
529 the *Fas2-B* isoform was amplified using isoform-specific oligonucleotides for *Fas2-B* (Fas2-F:
530 5´-TCATACTCGCATTCTCTCGC and Fas2B-R: 5´-TGATAATTTGTCAGCGGGAGG). PCR
531 products were cloned into pCR-BluntII-Topo vector using Zero Blunt Topo PCR Cloning Kit
532 (Thermo Fisher, 450245), sequenced, and subcloned into the EcoRI site in pUAST-attB. The
533 construct was integrated into the attP40/25C6 and attP2/68A4 landing sites.

534 **Antibodies and immunostainings**

535 Embryos were fixed in 4% formaldehyde in PBS/heptane for 20 minutes and devitellinized by
536 shaking in methanol/heptane. Ovaries were dissected in M3 insect medium (Sigma S8398)
537 and transferred into a 2 ml Eppendorf tube. For RUSH experiments, medium was removed
538 and 400 μl new M3 medium containing 1.5 mM Biotin was added for either 10 or 30 min. After

539 fixation for 10 min in 4% formaldehyde in PBS, ovaries were permeabilized by washing with
540 0.1% TritonX-100 in PBS (PBT), blocked for 20 min with 0.5% BSA in PBT, and then incubated
541 with primary antibodies for 3 h at room temperature. For detecting F-actin, Alexa Fluor 568-
542 Phalloidin (Thermo Fisher, A12380) was added at 1:100 dilution. After three washing steps,
543 ovaries were incubated for 2 h with secondary antibodies, washed and mounted in Vectashield
544 mouting medium.

545 The following antibodies were used: chicken anti-GFP (1:500; Abcam 13970), mouse anti-
546 GFP mAB 12A6 (1:300; DSHB), goat anti-GFP-FITC (1:100; GeneTex GTX26662-100),
547 mouse anti-mCherry (1:200; Biorbyt orb66657), rabbit anti-RFP (1:200; Rockland 600-401-
548 379), chicken anti-mCherry (1:1000; Novus NBP2-25158SS), mouse anti-Streptavidin (1:500;
549 Abcam S10D4, ab10020), rabbit anti-Streptavidin (1:200; Abcam ab6676), rabbit anti-Serp
550 (1:300; Luschnig et al., 2006), goat anti-Golgin245 (1:400; DSHB), mouse anti-Rab7 (1:20;
551 DSHB), mouse anti-KDEL (1:100; Abcam 10C3), rabbit anti-Dysfusion (1:500; Jiang and
552 Crews, 2003), rabbit-anti-Sec16 (1:1000; Ivan et al., 2008), mouse anti-Sxl M18-c (1:500;
553 DSHB), anti-Tango (1:200; DSHB). Goat secondary antibodies were conjugated with Alexa
554 Fluor 488, Alexa Fluor 568, Alexa Fluor 647 (Thermo Fisher), or Cy5 (Jackson
555 ImmunoResearch). Chitin was detected using AlexaFluor-labeled chitin-binding domain from
556 *Bacillus circulans* chitinase A1 as described in (Caviglia and Luschnig, 2013).

557 **Culture of ovarian follicles**

558 Adult females expressing Fas2::SVS (CPTI000483) and two copies of ST-KDEL in follicle cells
559 under the control of *GR1*-Gal4 were fed fresh yeast paste supplemented with Avidin (50 ppm;
560 Sigma A9275) at 27°C for two days after eclosion. Ovaries were dissected in M3 insect
561 medium containing 0.05% $KHCO_3$ and 1x penicillin/streptomycin (from 100x stock; Thermo
562 Fisher). To minimize biotin content of the medium, yeast extract and Bacto Peptone were not
563 added. CellMask Orange (Thermo Fisher) and Hoechst 33342 (Sigma) were added to the
564 medium to stain plasma membranes and nuclei, respectively. Dissected follicles were
565 transferred to 8-well glass-bottom chambers (VWR 734-2061) containing 200 µl M3 medium
566 per well. Before use, glass-bottom chambers were coated with poly-D-Lysine (Sigma P1024;
567 1 mg/ml in water, pH 8.5) for 1 h at 37°C to immobilize follicles on the glass surface. To induce
568 release of ER-retained proteins, 200 µl of M3 medium containing 3 mM biotin were added to
569 the culture medium (1.5 mM final biotin concentration) during imaging. For inducing ER stress,
570 Dithiothreitol (DTT; Roth 6908.2) was added to the culture medium (5 mM final concentration)
571 for 2.5 hours before imaging.

572 **Microscopy and embryo microinjections**

573 Imaging was performed using HyD detectors and 40x/1.3 NA and 63x/1.4 NA objectives on a
574 Leica SP8 inverted confocal microscope or using 40x/1.3 NA and 60x/1.35 NA objectives on
575 an Olympus FV1000 inverted confocal microscope. For live imaging, embryos (12-15 h AEL)
576 were dechorionated, placed on apple juice agar plates, and visually selected for ER retention
577 of GFP-tagged cargo proteins using a Leica M165 FC fluorescence stereomicroscope.
578 Selected embryos were transferred to glue-coated coverslips and covered with Voltalef 10S
579 halocarbon oil (VWR) before injection with D-biotin (B4501; Sigma-Aldrich) at the indicated
580 concentration (unless indicated otherwise, 1 mM in water). Biotin was injected ventrally into
581 the body cavity of embryos using either a Transjector 5246 microinjector (Eppendorf) with
582 Femtotips II at a transmitted light microscope or using a FemtoJet microinjector (Eppendorf)
583 mounted on an inverted Leica SP8 confocal microscope.

584 For high-resolution imaging of ER exit sites, living embryos were imaged using a 63x/1.4 NA
585 objective on a Leica SP8 confocal microscope. Images were processed by deconvolution with
586 Huygens Professional (Scientific Volume Imaging, The Netherlands, http://svi.nl) using the
587 CMLE algorithm with SNR:15 and 40 iterations.

588 For tracking Fas2::SVS vesicles in follicle cells, cultured egg chambers were imaged on an
589 inverted Leica SP5 confocal microscope using HyD detectors and a 63x/1.30 NA HCX PL
590 APO glycerol immersion objective. For time-lapse movies, images (512 x 256 pixels) were
591 acquired at 1 second time intervals.

592 **Image analysis**

593 Images were processed using Fiji/ImageJ (Schindelin et al., 2012), Imaris (v7.7.0; Bitplane),
594 OMERO (5.4.10; Allan et al., 2012), and Scikit-Image (v0.18.2; van der Walt et al., 2014).
595 Serp-SBG signals in tracheal cells and lumen were measured in manually selected regions of
596 interest (ROIs) on average-intensity projections of confocal sections acquired in tracheal DT
597 metamere 7. Background intensity was measured in the hemocoel outside the trachea and
598 was subtracted from intracellular and luminal signals. Serp-SBG-containing endosomal
599 vesicles were segmented by applying a median filter (radius 2.0) and a manual threshold.
600 Vesicle diameter (Feret distance) was measured using the Analyze Particles plugin in Fiji.
601 Vesicle velocity was measured using the Spots function in Imaris.

602 For analyzing the dynamics of Serp-SBG at ER exit sites, mCherry-Sec24-labeled ERES were
603 segmented using the Imaris 3D Spot function. Serp-SBG signals within spherical mCherry-
604 Sec24-containing volumes were measured in Imaris. To quantify the area of intersection
605 between mCherry-Sec24 and Serp-SBG signals at ERES, signals were segmented using
606 Default (for mCherry-Sec24) or Yen Fiji (for Serp-SBG) automatic threshold methods.

607 For analysis of tricellular junction assembly in embryonic epidermis, images were processed
608 by deconvolution and corrected for x-y drift using the CMLE algorithm in Huygens Professional
609 with SNR:10 for the CyPet-nls channel, SNR:8 for Gli::SVS and Dlg1::tagRFP channels, and
610 30 iterations (all channels). For quantifying Gli::SVS signals, mean gray values at TCJs, BCJs,
611 and inside cells were measured in manually selected ROIs for each time point on average-
612 intensity projections of the three most apical slices showing junctional signal in a z-stack. For
613 each time point, the mean intensity for TCJs and intracellular signals, respectively, was
614 calculated. Values were then normalized to the mean of the first three time points per group
615 (TCJs, BCJs, intracellular signals). To determine the apical-basal distribution of Gli::SVS along
616 vertices, Gli::SVS signals were analyzed in average-intensity projections of three vertical (x-
617 z) sections. Dlg1::tagRFP signals were used to manually trace vertices of control and ST-
618 KDEL-expressing cells. Gli::SVS signals were measured along a line (width = 10 pixels) drawn
619 along the Dlg1::tagRFP-marked vertex. Values for each junction were normalized to the
620 highest intensity value measured for the respective junction.

621 For quantifying nuclear Xbp1-GFP signals as a read-out of ER stress, nuclei were segmented
622 using Hoechst 33342 staining (for follicle cells in cultured egg chambers) or using nuclear
623 Tango staining (for tracheal cells in fixed embryos). A Median filter (radius = 8) was applied to
624 the nuclear signal, followed by image binarization using a Mean threshold. Small particles
625 were removed by size exclusion. Xbp1-GFP signals were measured within segmented nuclei
626 using FIJI (v2.3.0). Mean Xbp1-GFP intensities per nucleus and mean values of all nuclei per
627 sample were calculated using R. At least 20 nuclei per embryo and at least 8 nuclei per egg
628 chamber were analyzed.

629 Fas2::SVS vesicles were tracked using the FIJI Manual tracking plug-in. For illustration of
630 individual tracks, the tracks were recolored and then assembled according to their orientation
631 and size in a standardized epithelial cell using Adobe Illustrator.

632 **Statistics**

633 Statistical analyses were performed in Microsoft Excel 2010, OriginLab 8.5, or R (3.5.1) using
634 RStudio Interface (1.3.1093). Sample size (n) was not predetermined using statistical methods
635 but was assessed empirically by considering the variability of a given effect as determined by
636 the standard deviation. Experiments were considered independent if the specimens analyzed
637 were derived from different crosses. Investigators were not blinded to allocation during
638 experiments. The data was tested for normality using the Shapiro-Wilk test. Student's t-test
639 was used for normally distributed data. When the data was not normally distributed, the
640 Wilcoxon rank-sum test (R standard package) was used. P values were corrected for multiple

testing using the Bonferroni-Holm method (Holm, 1979). Sample size is indicated in the graphs or figure legends.

## Author contributions

Conceptualization, J.G., C.C., S.L.; Methodology, all authors; Investigation, J.G., C.C., M.H., J.I.S., T.J., W.B., N.B., V.R.; Formal Analysis, J.G., C.C., M.H., T.J., R.S., N.B., V.R; Visualization, J.G., C.C., M.H., T.J., W.B., N.B., V.R.; Reagents and tools, J.G., C.C., M.H., T.J., W.B., D.F., S.L.; Writing – Original Draft, J.G., C.C., S.L.; Writing – Review and Editing, C.C., S.L.; Funding Acquisition, V.R., S.L.; Supervision, S.L.

## Acknowledgements

We thank Franck Perez for advice and discussions, and Sarah Weischer and Thomas Zobel at the Münster Imaging Network for expert support with image analysis. N.B. and V.R. acknowledge support by the Core Facility Live Cell Imaging Mannheim (DFG INST 91027/9-1 FUGG).

## Funding

J.G. was supported by a Forschungskredit fellowship of the University of Zürich, where this work was initiated. Work in V.R.´s laboratory was funded by the German Research Foundation (DFG RI 1225/2-2). Work in S.L.'s laboratory was supported by the German Research Foundation (SFB 1348 "Dynamic Cellular Interfaces"; SFB 1009 "Breaking Barriers"), the "Cells-in-Motion" Cluster of Excellence (EXC 1003-CiM) at the University of Münster, and the University of Münster.

## Competing interests

The authors declare that they have no conflict of interest.

## References

**Allan, C., Burel, J. M., Moore, J., Blackburn, C., Linkert, M., Loynton, S., Macdonald, D., Moore, W. J., Neves, C., Patterson, A., et al.** (2012). OMERO: flexible, model-driven data management for experimental biology. *Nat Methods* **9**, 245–53.

673 **Armbruster, K. and Luschnig, S.** (2012). The Drosophila Sec7 domain guanine nucleotide exchange
674 factor protein Gartenzwerg localizes at the cis-Golgi and is essential for epithelial tube expansion.
675 *Journal of cell science* **125**, 1318–1328.

676 **Babatz, F., Naffin, E. and Klämbt, C.** (2018). The Drosophila Blood-Brain Barrier Adapts to Cell
677 Growth by Unfolding of Pre-existing Septate Junctions. *Dev Cell* **47**, 697-710.e3.

678 **Bannykh, S. I., Rowe, T. and Balch, W. E.** (1996). The organization of endoplasmic reticulum export
679 complexes. *J Cell Biol* **135**, 19–35.

680 **Barrette-Ng, I. H., Wu, S. C., Tjia, W. M., Wong, S. L. and Ng, K. K.** (2013). The structure of the SBP-
681 Tag-streptavidin complex reveals a novel helical scaffold bridging binding pockets on separate subunits.
682 *Acta crystallographica. Section D, Biological crystallography* **69**, 879–87.

683 **Bischof, J., Maeda, R. K., Hediger, M., Karch, F. and Basler, K.** (2007). An optimized transgenesis
684 system for Drosophila using germ-line-specific phiC31 integrases. *Proc Natl Acad Sci U S A* **104**, 3312–
685 7.

686 **Boncompain, G., Divoux, S., Gareil, N., de Forges, H., Lescure, A., Latreche, L., Mercanti, V.,**
687 **Jollivet, F., Raposo, G. and Perez, F.** (2012). Synchronization of secretory protein traffic in populations
688 of cells. *Nat Methods* **9**, 493–8.

689 **Brand, A. H. and Perrimon, N.** (1993). Targeted gene expression as a means of altering cell fates and
690 generating dominant phenotypes. *Development* **118**, 401–415.

691 **Casler, J. C., Zajac, A. L., Valbuena, F. M., Sparvoli, D., Jeyifous, O., Turkewitz, A. P., Horne-**
692 **Badovinac, S., Green, W. N. and Glick, B. S.** (2020). ESCargo: a regulatable fluorescent secretory
693 cargo for diverse model organisms. *MBoC* **31**, 2892–2903.

694 **Caussinus, E., Colombelli, J. and Affolter, M.** (2008). Tip-Cell Migration Controls Stalk-Cell
695 Intercalation during Drosophila Tracheal Tube Elongation. *Current Biology* **18**, 1727–1734.

696 **Caussinus, E., Kanca, O. and Affolter, M.** (2012). Fluorescent fusion protein knockout mediated by
697 anti-GFP nanobody. *Nat Struct Mol Biol* **19**, 117–21.

698 **Caviglia, S. and Luschnig, S.** (2013). The ETS domain transcriptional repressor Anterior open inhibits
699 MAP kinase and Wingless signaling to couple tracheal cell fate with branch identity. *Development* **140**,
700 1240–9.

701 **Caviglia, S., Brankatschk, M., Fischer, E. J., Eaton, S. and Luschnig, S.** (2016). Staccato/Unc-13-
702 4 controls secretory lysosome-mediated lumen fusion during epithelial tube anastomosis. *Nat Cell Biol*
703 **18**, 727–39.

704 **Chen, D., Gibson, E. S. and Kennedy, M. J.** (2013). A light-triggered protein secretion system. *Journal*
705 *of Cell Biology* **201**, 631–640.

706 **Chow, C. Y., Avila, F. W., Clark, A. G. and Wolfner, M. F.** (2015). Induction of Excessive Endoplasmic
707 Reticulum Stress in the Drosophila Male Accessory Gland Results in Infertility. *PLoS ONE* **10**,
708 e0119386.

709 **Dong, B., Kakihara, K., Otani, T., Wada, H. and Hayashi, S.** (2013). Rab9 and retromer regulate
710 retrograde trafficking of luminal protein required for epithelial tube length control. *Nat Commun* **4**, 1358.

711 **Förster, D., Armbruster, K. and Luschnig, S.** (2010). Sec24-dependent secretion drives cell-
712 autonomous expansion of tracheal tubes in Drosophila. *Curr Biol* **20**, 62–8.

713 **Fourriere, L., Divoux, S., Roceri, M., Perez, F. and Boncompain, G.** (2016). Microtubule-independent
714 secretion requires functional maturation of Golgi elements. *J Cell Sci* **129**, 3238–3250.

715 **Griffiths, G., Pfeiffer, S., Simons, K. and Matlin, K.** (1985). Exit of newly synthesized membrane
716 proteins from the trans cisterna of the Golgi complex to the plasma membrane. *J Cell Biol* **101**, 949–
717 964.

718 **Harmansa, S., Alborelli, I., Bieli, D., Caussinus, E. and Affolter, M.** (2017). A nanobody-based
719 toolset to investigate the role of protein localization and dispersal in Drosophila. *Elife* **6**, e22549.

720 **Hetz, C., Zhang, K. and Kaufman, R. J.** (2020). Mechanisms, regulation and functions of the unfolded
721 protein response. *Nat Rev Mol Cell Biol* **21**, 421–438.

722 **Holm, S.** (1979). A Simple Sequentially Rejective Multiple Test Procedure. *Scandinavian Journal of*
723 *Statistics* **6**, 65–70.

724 **Ikeya, T. and Hayashi, S.** (1999). Interplay of Notch and FGF signaling restricts cell fate and MAPK
725 activation in the Drosophila trachea. *Development* **126**, 4455–4463.

726 **Ivan, V., de Voer, G., Xanthakis, D., Spoorendonk, K. M., Kondylis, V. and Rabouille, C.** (2008).
727 Drosophila Sec16 Mediates the Biogenesis of tER Sites Upstream of Sar1 through an Arginine-Rich
728 Motif. *Mol Biol Cell* **19**, 4352–4365.

729 **Jiang, L. and Crews, S. T.** (2003). The Drosophila dysfusion Basic Helix-Loop-Helix (bHLH)-PAS Gene
730 Controls Tracheal Fusion and Levels of the Trachealess bHLH-PAS Protein. *Molecular and Cellular*
731 *Biology* **23**, 5625–5637.

732 **Keefe, A. D., Wilson, D. S., Seelig, B. and Szostak, J. W.** (2001). One-step purification of recombinant
733 proteins using a nanomolar-affinity streptavidin-binding peptide, the SBP-Tag. *Protein Expr Purif* **23**,
734 440–6.

735 **Kim, J. H., Chang, T. M., Graham, A. N., Andy Choo, K. H., Kalitsis, P. and Hudson, D. F.** (2010).
736 Streptavidin-Binding Peptide (SBP)-tagged SMC2 allows single-step affinity fluorescence, blotting or
737 purification of the condensin complex. *BMC Biochemistry* **11**, 50.

738 **Kondylis, V. and Rabouille, C.** (2009). The Golgi apparatus: lessons from Drosophila. *FEBS Lett* **583**,
739 3827–38.

740 **Kreis, T. E. and Lodish, H. F.** (1986). Oligomerization is essential for transport of vesicular stomatitis
741 viral glycoprotein to the cell surface. *Cell* **46**, 929–37.

742 **Lafay, F.** (1974). Envelope proteins of vesicular stomatitis virus: effect of temperature-sensitive
743 mutations in complementation groups III and V. *J Virol* **14**, 1220–8.

744 **Le, T., Liang, Z., Patel, H., Yu, M. H., Sivasubramaniam, G., Slovitt, M., Tanentzapf, G., Mohanty,**
745 **N., Paul, S. M., Wu, V. M., et al.** (2006). A new family of Drosophila balancer chromosomes with a w-
746 dfd-GMR yellow fluorescent protein marker. *Genetics* **174**, 2255–2257.

747 **Lippincott-Schwartz, J., Yuan, L. C., Bonifacino, J. S. and Klausner, R. D.** (1989). Rapid
748 redistribution of Golgi proteins into the ER in cells treated with brefeldin A: evidence for membrane
749 cycling from Golgi to ER. *Cell* **56**, 801–813.

750 **Llimargas, M.** (1999). The Notch pathway helps to pattern the tips of the Drosophila tracheal branches
751 by selecting cell fates. *Development* **126**, 2355–2364.

752 **Lowe, N., Rees, J. S., Roote, J., Ryder, E., Armean, I. M., Johnson, G., Drummond, E., Spriggs,**

**H., Drummond, J., Magbanua, J. P., et al.** (2014). Analysis of the expression patterns, subcellular localisations and interaction partners of Drosophila proteins using a pigP protein trap library. *Development* **141**, 3994–4005.

**Luschnig, S., Bätz, T., Armbruster, K. and Krasnow, M. A.** (2006). serpentine and vermiform encode matrix proteins with chitin binding and deacetylation domains that limit tracheal tube length in Drosophila. *Curr Biol* **16**, 186–94.

**Lye, C. M., Naylor, H. W. and Sanson, B.** (2014). Subcellular localisations of the CPTI collection of YFP-tagged proteins in Drosophila embryos. *Development* **141**, 4006–17.

**Matsuda, S., Schaefer, J. V., Mii, Y., Hori, Y., Bieli, D., Taira, M., Plückthun, A. and Affolter, M.** (2021). Asymmetric requirement of Dpp/BMP morphogen dispersal in the Drosophila wing disc. *Nat Commun* **12**, 6435.

**McGuire, S. E., Mao, Z. and Davis, R. L.** (2004). Spatiotemporal gene expression targeting with the TARGET and gene-switch systems in Drosophila. *Sci STKE* **2004**, pl6.

**Mehta, A. D., Rock, R. S., Rief, M., Spudich, J. A., Mooseker, M. S. and Cheney, R. E.** (1999). Myosin-V is a processive actin-based motor. *Nature* **400**, 590–593.

**Meinken, J., Walker, G., Cooper, C. R. and Min, X. J.** (2015). MetazSecKB: the human and animal secretome and subcellular proteome knowledgebase. *Database* **2015**, bav077.

**Nelson, J. O., Förster, D., Frizzell, K. A., Luschnig, S. and Metzstein, M. M.** (2018). Multiple Nonsense-Mediated mRNA Processes Require Smg5 in Drosophila. *Genetics* **209**, 1073–1084.

**Neuert, H., Deing, P., Krukkert, K., Naffin, E., Steffes, G., Risse, B., Silies, M. and Klämbt, C.** (2020). The *Drosophila* NCAM homolog Fas2 signals independently of adhesion. *Development* **147**, dev181479.

**Pei, J., Kinch, L. N. and Grishin, N. V.** (2018). FlyXCDB—A Resource for Drosophila Cell Surface and Secreted Proteins and Their Extracellular Domains. *Journal of Molecular Biology* **430**, 3353–3411.

**Pinheiro, D., Hannezo, E., Herszterg, S., Bosveld, F., Gaugue, I., Balakireva, M., Wang, Z., Cristo, I., Rigaud, S. U., Markova, O., et al.** (2017). Transmission of cytokinesis forces via E-cadherin dilution and actomyosin flows. *Nature* **545**, 103–107.

**Presley, J. F., Cole, N. B., Schroer, T. A., Hirschberg, K., Zaal, K. J. and Lippincott-Schwartz, J.** (1997). ER-to-Golgi transport visualized in living cells. *Nature* **389**, 81–85.

**Reynolds, H. M., Zhang, L., Tran, D. T. and Ten Hagen, K. G.** (2019). Tango1 coordinates the formation of endoplasmic reticulum/Golgi docking sites to mediate secretory granule formation. *J Biol Chem* **294**, 19498–19510.

**Rollins, C. T., Rivera, V. M., Woolfson, D. N., Keenan, T., Hatada, M., Adams, S. E., Andrade, L. J., Yaeger, D., van Schravendijk, M. R., Holt, D. A., et al.** (2000). A ligand-reversible dimerization system for controlling protein–protein interactions. *Proceedings of the National Academy of Sciences* **97**, 7096–7101.

**Ryoo, H. D.** (2015). Drosophila as a model for unfolded protein response research. *BMB Reports* **48**, 445–453.

**Ryoo, H. D., Domingos, P. M., Kang, M.-J. and Steller, H.** (2007). Unfolded protein response in a Drosophila model for retinal degeneration. *EMBO J* **26**, 242–252.

**Sauerwald, J., Soneson, C., Robinson, M. D. and Luschnig, S.** (2017). Faithful mRNA splicing depends on the Prp19 complex subunit faint sausage and is required for tracheal branching morphogenesis in Drosophila. *Development* **144**, 657–663.

**Scales, S. J., Pepperkok, R. and Kreis, T. E.** (1997). Visualization of ER-to-Golgi transport in living cells reveals a sequential mode of action for COPII and COPI. *Cell* **90**, 1137–48.

**Schindelin, J., Arganda-Carreras, I., Frise, E., Kaynig, V., Longair, M., Pietzsch, T., Preibisch, S., Rueden, C., Saalfeld, S., Schmid, B., et al.** (2012). Fiji: an open-source platform for biological-image analysis. *Nature Methods* **9**, 676–682.

**Schotman, H. and Rabouille, C.** (2009). The Exocytic Pathway and Development. In *Trafficking Inside Cells*, pp. 419–438. New York, NY: Springer New York.

**Schweizer, A., Fransen, J. A., Matter, K., Kreis, T. E., Ginsel, L. and Hauri, H. P.** (1990). Identification of an intermediate compartment involved in protein transport from endoplasmic reticulum to Golgi apparatus. *Eur J Cell Biol* **53**, 185–196.

**Shomron, O., Nevo-Yassaf, I., Aviad, T., Yaffe, Y., Zahavi, E. E., Dukhovny, A., Perlson, E., Brodsky, I., Yeheskel, A., Pasmanik-Chor, M., et al.** (2021). COPII collar defines the boundary between ER and ER exit site and does not coat cargo containers. *J Cell Biol* **220**, e201907224.

**Sone, M., Zeng, X., Larese, J. and Ryoo, H. D.** (2013). A modified UPR stress sensing system reveals a novel tissue distribution of IRE1/XBP1 activity during normal Drosophila development. *Cell Stress and Chaperones* **18**, 307–319.

**Stalder, D. and Gershlick, D. C.** (2020). Direct trafficking pathways from the Golgi apparatus to the plasma membrane. *Semin Cell Dev Biol* **107**, 112–125.

**Steneberg, P., Hemphälä, J. and Samakovlis, C.** (1999). Dpp and Notch specify the fusion cell fate in the dorsal branches of the Drosophila trachea. *Mech Dev* **87**, 153–163.

**Subramanian, A., Capalbo, A., Iyengar, N. R., Rizzo, R., di Campli, A., Di Martino, R., Lo Monte, M., Beccari, A. R., Yerudkar, A., del Vecchio, C., et al.** (2019). Auto-regulation of Secretory Flux by Sensing and Responding to the Folded Cargo Protein Load in the Endoplasmic Reticulum. *Cell* **176**, 1461-1476.e23.

**Terai, T., Maki, E., Sugiyama, S., Takahashi, Y., Matsumura, H., Mori, Y. and Nagano, T.** (2011). Rational development of caged-biotin protein-labeling agents and some applications in live cells. *Chem Biol* **18**, 1261–72.

**Tsarouhas, V., Senti, K. A., Jayaram, S. A., Tiklová, K., Hemphälä, J., Adler, J. and Samakovlis, C.** (2007). Sequential pulses of apical epithelial secretion and endocytosis drive airway maturation in Drosophila. *Dev Cell* **13**, 214–25.

**van der Walt, S., Schönberger, J. L., Nunez-Iglesias, J., Boulogne, F., Warner, J. D., Yager, N., Gouillart, E., Yu, T., and scikit-image contributors** (2014). scikit-image: image processing in Python. *PeerJ* **2**, e453.

**Venken, K. J., Schulze, K. L., Haelterman, N. A., Pan, H., He, Y., Evans-Holm, M., Carlson, J. W., Levis, R. W., Spradling, A. C., Hoskins, R. A., et al.** (2011). MiMIC: a highly versatile transposon insertion resource for engineering Drosophila melanogaster genes. *Nat Methods* **8**, 737–43.

**Voss, S. and Skerra, A.** (1997). Mutagenesis of a flexible loop in streptavidin leads to higher affinity for the Strep-tag II peptide and improved performance in recombinant protein purification. *Protein Eng* **10**, 975–82.

**Wang, S., Jayaram, S. A., Hemphälä, J., Senti, K. A., Tsarouhas, V., Jin, H. and Samakovlis, C.** (2006). Septate-junction-dependent luminal deposition of chitin deacetylases restricts tube elongation in the Drosophila trachea. *Curr Biol* **16**, 180–5.

**Weigel, A. V., Chang, C.-L., Shtengel, G., Xu, C. S., Hoffman, D. P., Freeman, M., Iyer, N., Aaron, J., Khuon, S., Bogovic, J., et al.** (2021). ER-to-Golgi protein delivery through an interwoven, tubular network extending from ER. *Cell* **184**, 2412-2429.e16.

**Westrate, L. M., Hoyer, M. J., Nash, M. J. and Voeltz, G. K.** (2020). Vesicular and uncoated Rab1-dependent cargo carriers facilitate ER to Golgi transport. *J Cell Sci* **133**, jcs239814.

**Wittek, A., Hollmann, M., Schleutker, R. and Luschnig, S.** (2020). The Transmembrane Proteins M6 and Anakonda Cooperate to Initiate Tricellular Junction Assembly in Epithelia of Drosophila. *Curr Biol* **30**, 4254-4262.e5.

**Yang, K., Liu, M., Feng, Z., Rojas, M., Zhou, L., Ke, H. and Pastor-Pareja, J. C.** (2021). ER exit sites in Drosophila display abundant ER-Golgi vesicles and pearled tubes but no megacarriers. *Cell Reports* **36**,.

**Yano, H., Yamamoto-Hino, M., Abe, M., Kuwahara, R., Haraguchi, S., Kusaka, I., Awano, W., Kinoshita-Toyoda, A., Toyoda, H. and Goto, S.** (2005). Distinct functional units of the Golgi complex in Drosophila cells. *Proc Natl Acad Sci U S A* **102**, 13467–72.

**Yarwood, R., Hellicar, J., Woodman, P. G. and Lowe, M.** (2020). Membrane trafficking in health and disease. *Disease Models & Mechanisms* **13**, dmm043448.

Figure 1

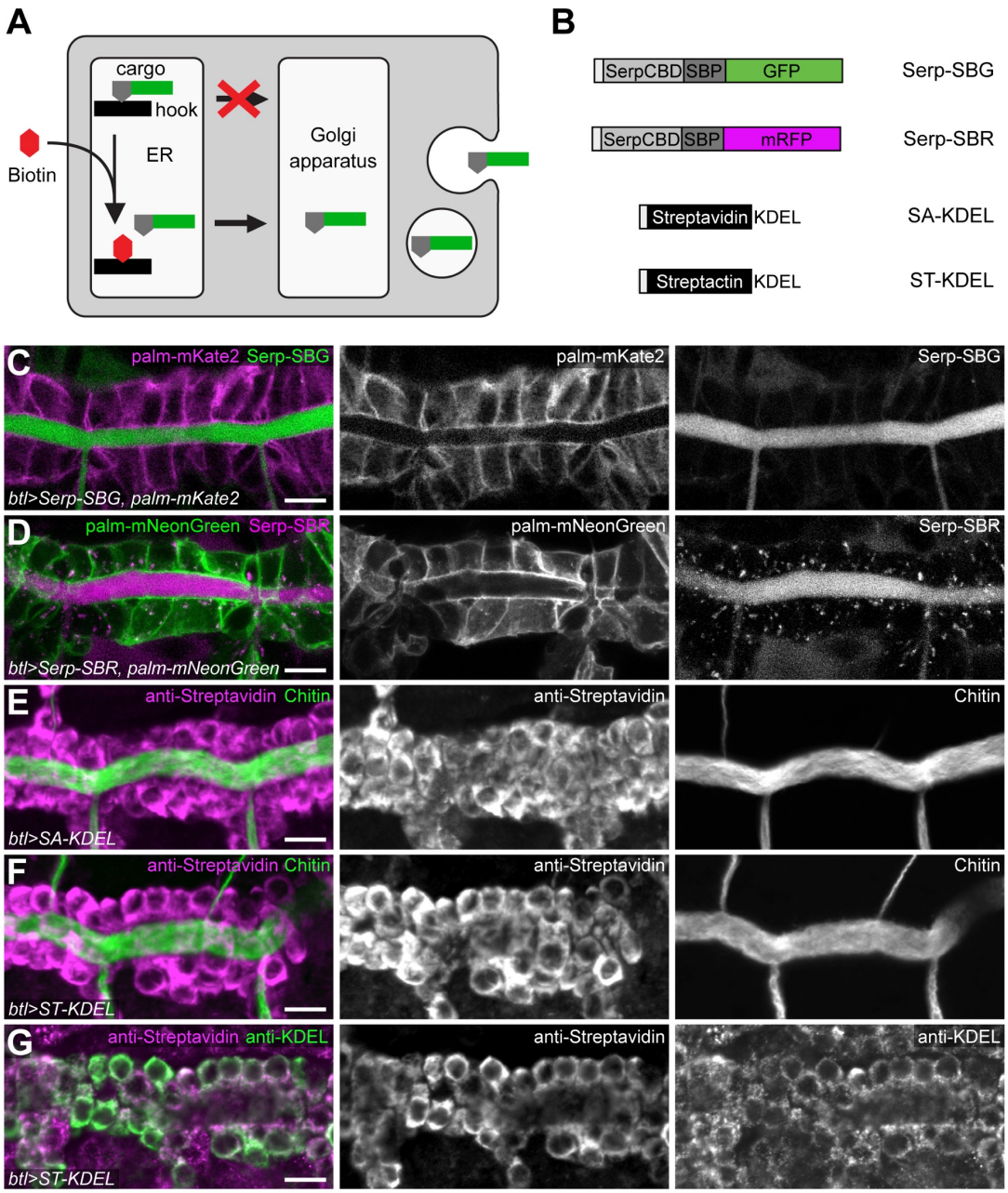
A
cargo
hook
ER
Biotin
Golgi apparatus
B
SerpCBD
SBP
GFP
Serp-SBG
SerpCBD
SBP
mRFP
Serp-SBR
Streptavidin
KDEL
SA-KDEL
Streptactin
KDEL
ST-KDEL
C
palm-mKate2 Serp-SBG
btl>Serp-SBG, palm-mKate2
palm-mKate2
Serp-SBG
D
palm-mNeonGreen Serp-SBR
btl>Serp-SBR, palm-mNeonGreen
palm-mNeonGreen
Serp-SBR
E
anti-Streptavidin Chitin
btl>SA-KDEL
anti-Streptavidin
Chitin
F
anti-Streptavidin Chitin
btl>ST-KDEL
anti-Streptavidin
Chitin
G
anti-Streptavidin anti-KDEL
btl>ST-KDEL
anti-Streptavidin
anti-KDEL

855

856 **Figure 1**

857 **A two-component system for controlling secretory protein trafficking *in vivo*.**

858 **(A)** Principle of RUSH. A streptavidin "hook" protein carrying an ER-retention signal is retained
859 in the ER lumen and binds a secretory cargo protein tagged with a fluorescent protein and a
860 Streptavidin-binding peptide (SBP), leading to ER retention of the cargo. Addition of biotin
861 dissociates the hook-cargo complex, thus allowing cargo to exit the ER and synchronizing the
862 passage of cargo through the secretory apparatus.

863 **(B)** Secretory cargo and ER-resident "hook" constructs. Cargo proteins consist of the N-
864 terminal signal peptide and chitin-binding domain of Serpentine (Serp-CBD) fused to a
865 Streptavidin-binding peptide (SBP) and a C-terminal EGFP (Serp-SBG, green) or mRFP
866 (Serp-SBR, magenta) tag. ER-resident hook proteins comprise either core streptavidin (SA)
867 or Streptactin (ST) fused to an N-terminal signal peptide and a C-terminal KDEL sequence.

868 **(C,D)** Confocal sections of tracheal dorsal trunk (metamere seven) in living embryos
869 expressing Serp-SBG (green; C) and palmitoylated mKate2 (palm-mKate2; magenta; C) or
870 Serp-SBR (magenta; D) and palmitoylated mNeonGreen (palm-mNeonGreen; green, D) in
871 tracheal cells under control of *btl*-Gal4. Anterior is to the left and dorsal is up here and in all
872 subsequent panels, unless noted otherwise.

873 **(E,F)** Confocal sections of tracheal dorsal trunk in fixed embryos expressing streptavidin-
874 KDEL (SA-KDEL; magenta, E) or Streptactin-KDEL (ST-KDEL; magenta, F) in tracheal cells,
875 stained with antibodies against streptavidin (magenta) and for chitin (tracheal lumen, green).

876 **(G)** Confocal section of tracheal dorsal trunk in embryo expressing Streptactin-KDEL, stained
877 with anti-streptavidin (magenta) and anti-KDEL (green) antibodies to label ER. Note
878 localization of ST-KDEL in the ER.

879 Scale bar: (C-G), 5 µm.

Figure 2

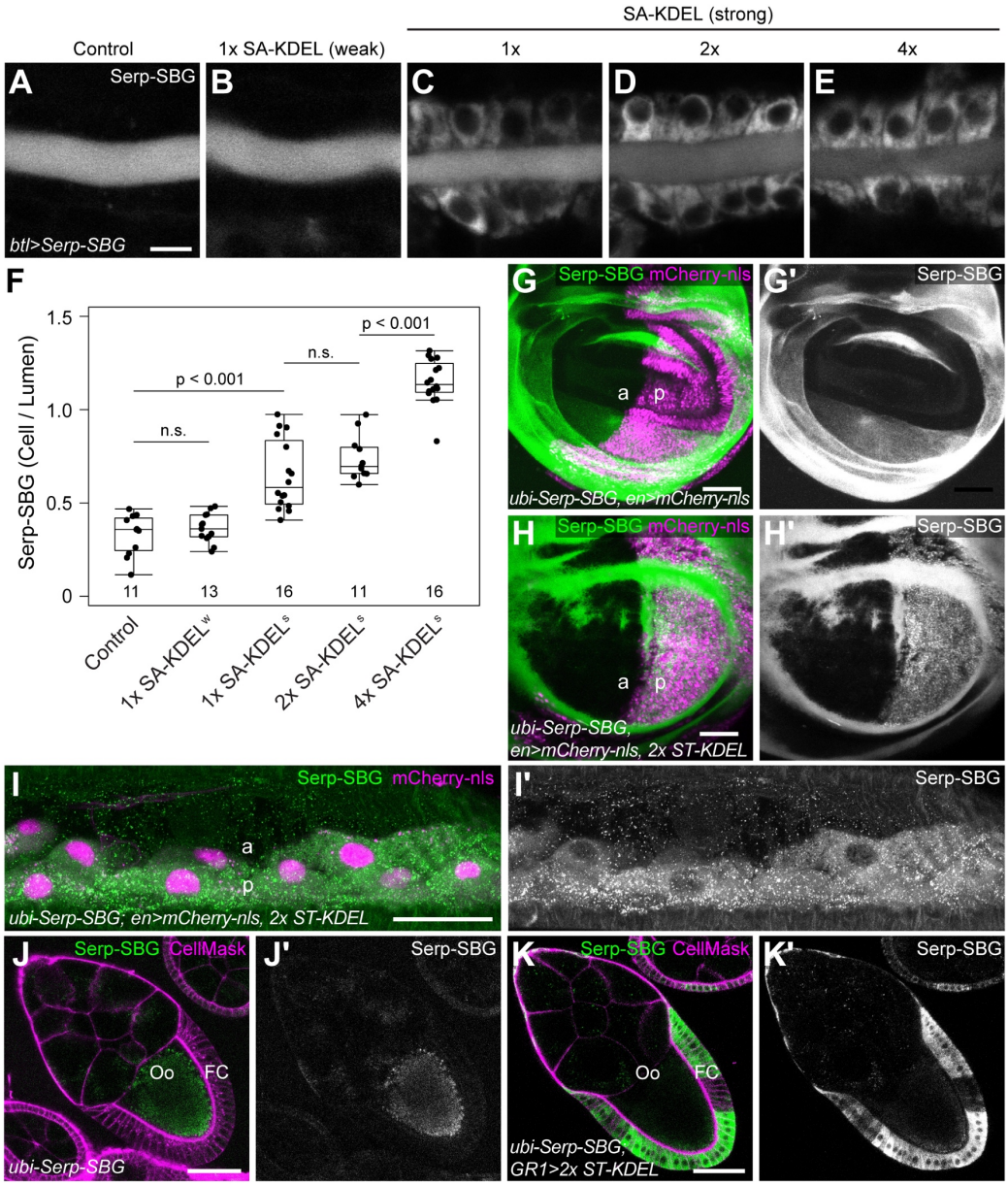
SA-KDEL (strong)
Control
1x SA-KDEL (weak)
1x
2x
4x
A
Serp-SBG
btl>Serp-SBG
B
C
D
E
F
Serp-SBG (Cell / Lumen)
1.5
1.0
0.5
0
p < 0.001
n.s.
p < 0.001
n.s.
11
13
16
11
16
Control
1x SA-KDEL^w
1x SA-KDEL^s
2x SA-KDEL^s
4x SA-KDEL^s
G
Serp-SBG mCherry-nls
a
p
ubi-Serp-SBG, en>mCherry-nls
G'
Serp-SBG
H
Serp-SBG mCherry-nls
a
p
ubi-Serp-SBG,
en>mCherry-nls, 2x ST-KDEL
H'
Serp-SBG
I
Serp-SBG mCherry-nls
a
p
ubi-Serp-SBG, en>mCherry-nls, 2x ST-KDEL
I'
Serp-SBG
J
Serp-SBG CellMask
Oo
FC
ubi-Serp-SBG
J'
Serp-SBG
K
Serp-SBG CellMask
Oo
FC
ubi-Serp-SBG,
GR1>2x ST-KDEL
K'
Serp-SBG

881 **Figure 2**

882 **The efficiency of ER retention depends on the ratio of cargo to hook proteins.**

883 **(A-E)** Confocal sections of dorsal trunk in living embryos (stage 15) expressing Serp-SBG
884 alone (control; A), with one copy of SA-KDEL(weak) (B), or with the indicated number of copies
885 of SA-KDEL(strong) (C-E) in tracheal cells. Note that intracellular Serp-SBG signals increase,
886 and luminal signals decrease with increasing dosage of SA-KDEL.

887 **(F)** Quantification of the ratio of intracellular and luminal Serp-SBG signals. Number of
888 embryos analyzed per genotype is indicated. Boxplot shows median (line), interquartile range
889 (box) and 1.5x interquartile range from the 25th and 75th percentile (whiskers). p-values
890 (Student´s t-test) are indicated; n.s., not significant.

891 **(G-H')** Wing imaginal discs of third-instar larvae expressing Serp-SBG (green) ubiquitously
892 under control of the *ubiquitin* (*ubi*) promoter. mCherry-nls (magenta) expression under control
893 of *en*-Gal4 marks the posterior compartment. In control disc (G,G'), Serp-SBG accumulates
894 in the disc lumen. Expression of ST-KDEL (two copies) in the posterior compartment leads to
895 intracellular retention of Serp-SBG in ST-KDEL-expressing cells (H,H'). a, anterior
896 compartment; p, posterior compartment.

897 **(I,I')** Epidermis of third-instar larvae expressing Serp-SBG (green) ubiquitously as in (G,H).
898 *en*-Gal4 drives expression of mCherry-nls (magenta) and ST-KDEL (two copies) in posterior
899 (p) compartment cells. Note diffuse distribution of Serp-SBG in cuticle of anterior (a)
900 compartment and intracellular retention in posterior compartment cells. Anterior is up.

901 **(J-K')** Ovarian egg chambers (stage 10A) from adult females expressing Serp-SBG (green)
902 ubiquitously under control of the *ubi* promoter. CellMask (magenta) marks plasma
903 membranes. In control egg chamber (J,J'), Serp-SBG is secreted by follicle cells (FC) and
904 taken up into the oocyte (Oo). Expression of ST-KDEL (two copies) in follicle cells driven by
905 GR1-Gal4 leads to intracellular retention of Serp-SBG (K,K'). Anterior is to upper left.

906 Scale bars: (A-E), 5 µm; (G-K), 50 µm.

Figure 3

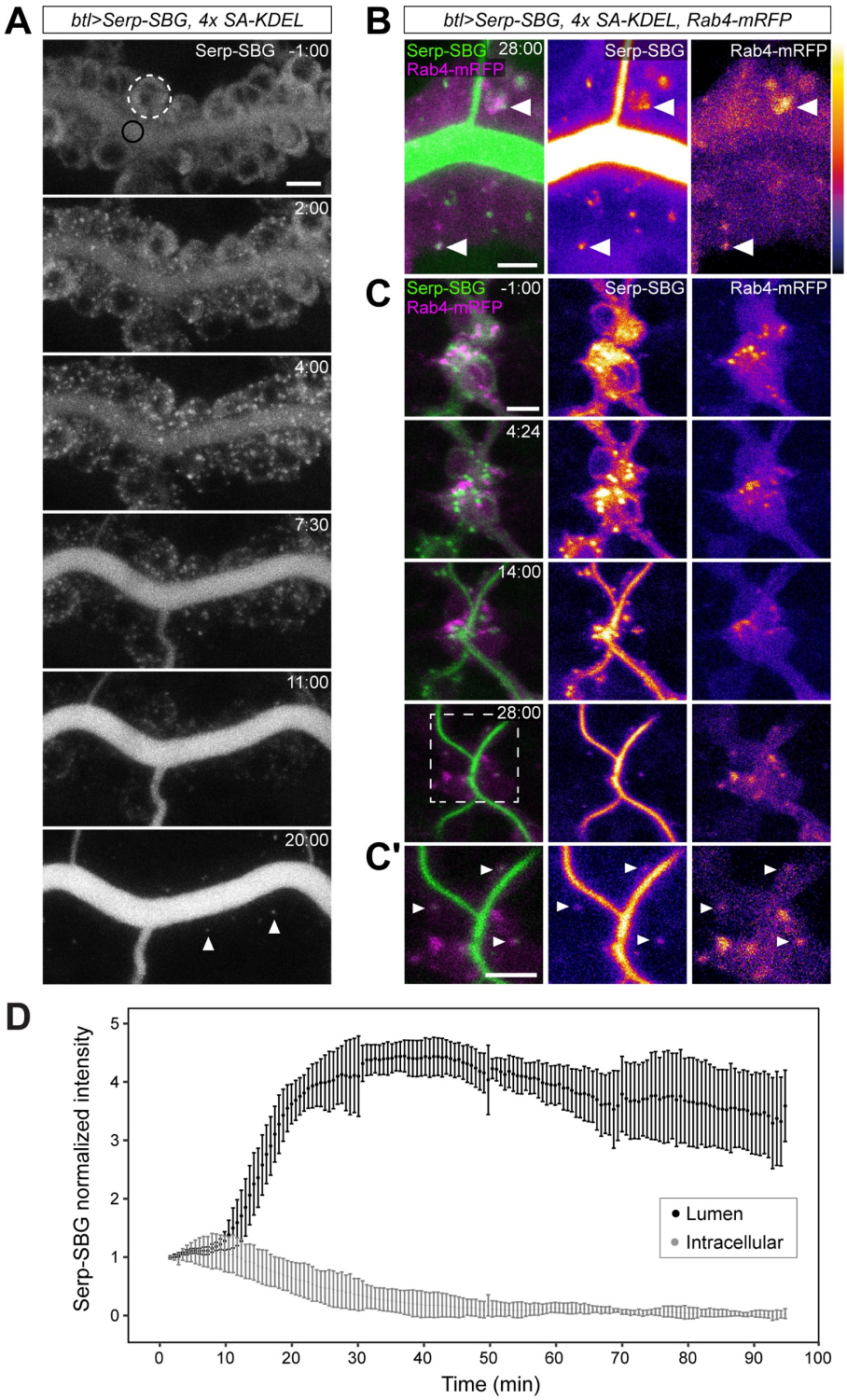
A
btl>Serp-SBG, 4x SA-KDEL
Serp-SBG -1:00
2:00
4:00
7:30
11:00
20:00
B
btl>Serp-SBG, 4x SA-KDEL, Rab4-mRFP
Serp-SBG 28:00
Rab4-mRFP
Serp-SBG
Rab4-mRFP
C
Serp-SBG -1:00
Rab4-mRFP
Serp-SBG
Rab4-mRFP
4:24
14:00
28:00
C'
D
Serp-SBG normalized intensity
Time (min)
Lumen
Intracellular

908 **Figure 3**

909 **Biotin injection triggers rapid ER exit and exocytosis of Serp-SBG in tracheal cells.**

910 **(A)** Stills (maximum-intensity projections) from time-lapse movie of embryo (stage 15)
911 expressing Serp-SBG and SA-KDEL (four copies) in tracheal cells. After biotin injection (1
912 mM) at t=0 min, Serp-SBG is released from ER, begins to accumulate at immobile puncta (ER
913 exit sites) 2 min after injection, and is subsequently secreted into the lumen. Rapidly moving
914 intracellular Serp-SBG-positive puncta, corresponding to endosomes, appear 20 min after
915 injection (arrowheads). ROIs in tracheal cells (dashed white circle) and lumen (black circle)
916 are indicated in top panel. Time (min:s) is indicated. See Movie S1.

917 **(B)** Confocal section of dorsal trunk in embryo (stage 15) expressing Serp-SBG, Rab4-mRFP
918 and SA-KDEL (four copies) in tracheal cells, 28 min after biotin injection. A subset of
919 intracellular Serp-SBG puncta overlaps with recycling endosomes marked by Rab4-mRFP
920 (arrowheads). Single-channel images display Serp-SBG and Rab4-mRFP intensities as a heat
921 map. Time (min:s) is indicated. See Movie S2.

922 **(C,C')** Stills (maximum-intensity projections) of dorsal branch from time-lapse movie of embryo
923 (stage 16) expressing Serp-SBG, Rab4-mRFP and SA-KDEL (four copies) in tracheal cells.
924 After injection of biotin at t=0 min, Serp-SBG is rapidly secreted into the lumen. At t=28 min,
925 Serp-SBG is detectable in recycling endosomes marked by Rab4-mRFP (C', arrowheads).
926 Anterior is to the left. Time (min:s) is indicated. See Movie S3.

927 **(D)** Quantification of Serp-SBG intensity in the lumen (black) and inside tracheal cells (grey)
928 of dorsal trunk after biotin injection at t=0 min. Mean intensities ± s.d., normalized to intensities
929 at t=0 min, are shown. n=5 embryos.

930 Scale bars: (A,B,C,C'), 5 μm.

# Figure 4

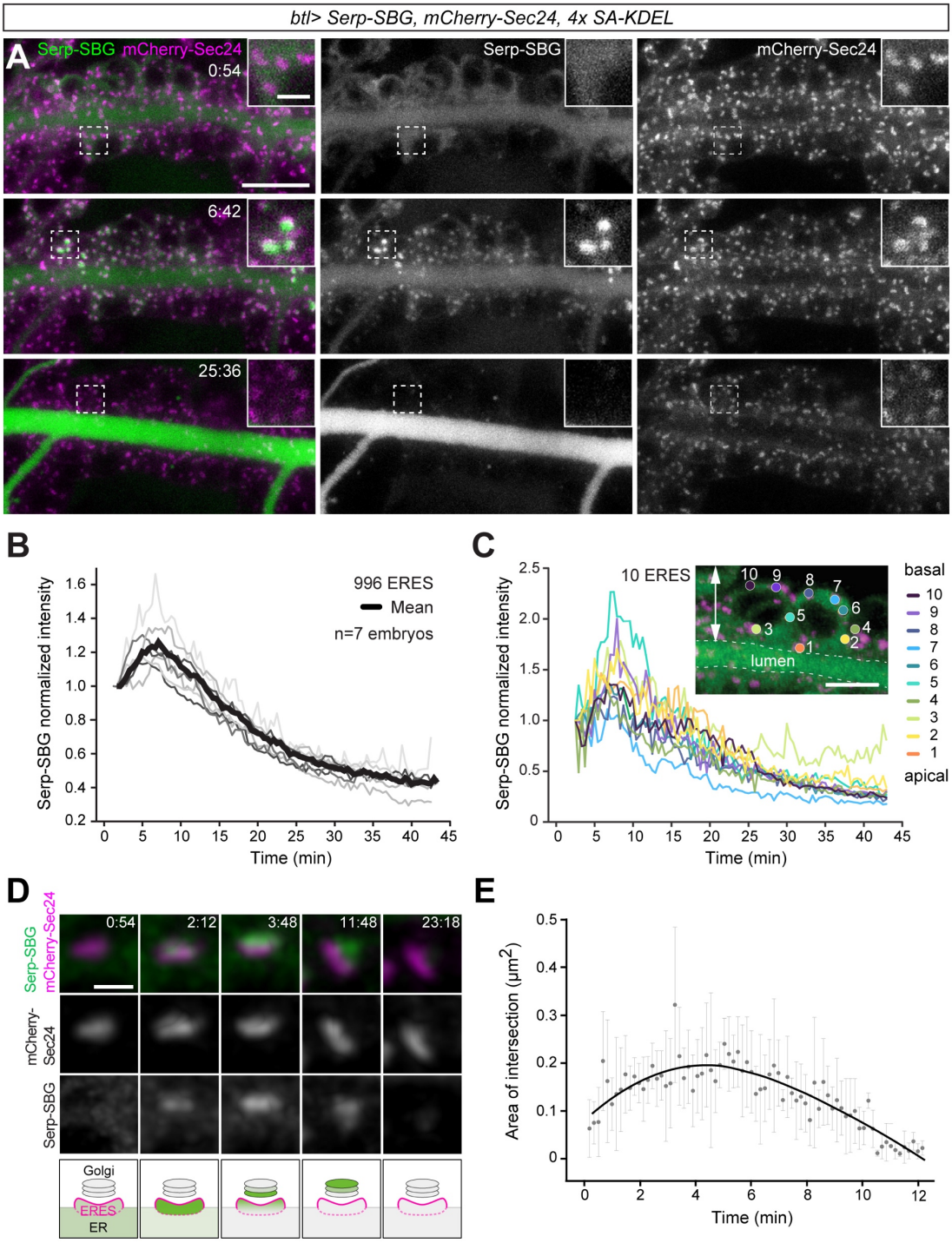
btl> Serp-SBG, mCherry-Sec24, 4x SA-KDEL
A
Serp-SBG mCherry-Sec24
0:54
6:42
25:36
Serp-SBG
mCherry-Sec24
B
996 ERES
Mean
n=7 embryos
Serp-SBG normalized intensity
Time (min)
C
10 ERES
lumen
basal
apical
Serp-SBG normalized intensity
Time (min)
D
Serp-SBG
mCherry-Sec24
0:54
2:12
3:48
11:48
23:18
mCherry-Sec24
Serp-SBG
Golgi
ERES
ER
E
Area of intersection (μm²)
Time (min)

932 **Figure 4**

933 **Rapid ER exit and passage of the Golgi apparatus by Serp-SBG.**

934 **(A)** Stills from time-lapse movie of tracheal dorsal trunk in embryo (stage 15) expressing Serp-
935 SBG, mCherry-Sec24 and four copies of SA-KDEL in tracheal cells. Biotin was injected at t=0
936 min. Serp-SBG (green) accumulates at ER exit-sites (mCherry-Sec24, magenta) at t=6:42.
937 Time (min:s) is indicated. See Movie S5.

938 **(B)** Quantification of Serp-SBG signals at mCherry-Sec24-positive ERES. Each thin line
939 indicates the mean of Serp-SBG intensity of at least 26 ERES per time point in one embryo,
940 thick black line shows the mean of seven embryos. Data were normalized to mean intensities
941 at the first time point. Serp-SBG accumulation at ERES is maximal seven minutes after biotin
942 injection.

943 **(C)** Quantification of Serp-SBG levels at ten ERES distributed from apical (1) to basal (10) in
944 tracheal cells indicates similar profiles of Serp-SBG trafficking.

945 **(D)** High-resolution images showing Serp-SBG (green) at a single mCherry-Sec24-labeled
946 ERES (magenta) after biotin injection at t=0 min. After ER release, Serp-SBG colocalizes with
947 mCherry-Sec24 (t=2:12) and subsequently shifts next to the mCherry-Sec24-marked ERES,
948 presumably residing in the Golgi apparatus (t=3:48, 11:48), before disappearing from the
949 ERES-Golgi complex (t=23:18). Images were processed using deconvolution. See Movie S6.
950 Scheme (bottom panel) illustrates passage of Serp-SBG (green) through the ERES (magenta)
951 and Golgi apparatus (grey). See Movie S6.

952 **(E)** Quantification of the area of intersection between Serp-SBG and mCherry-Sec24. Each
953 data point represents the mean ± s.d. of the overlapping area between Serp-SBG and
954 mCherry-Sec24 signals. Between 38 and 58 mCherry-Sec24-positive ERES were analyzed
955 per time point. The black curve shows a local polynomial regression fit.

956 Scale bars: (A), 10 µm, insets: 2 µm; (C), 5 µm; (D) 1 µm.

Figure 5

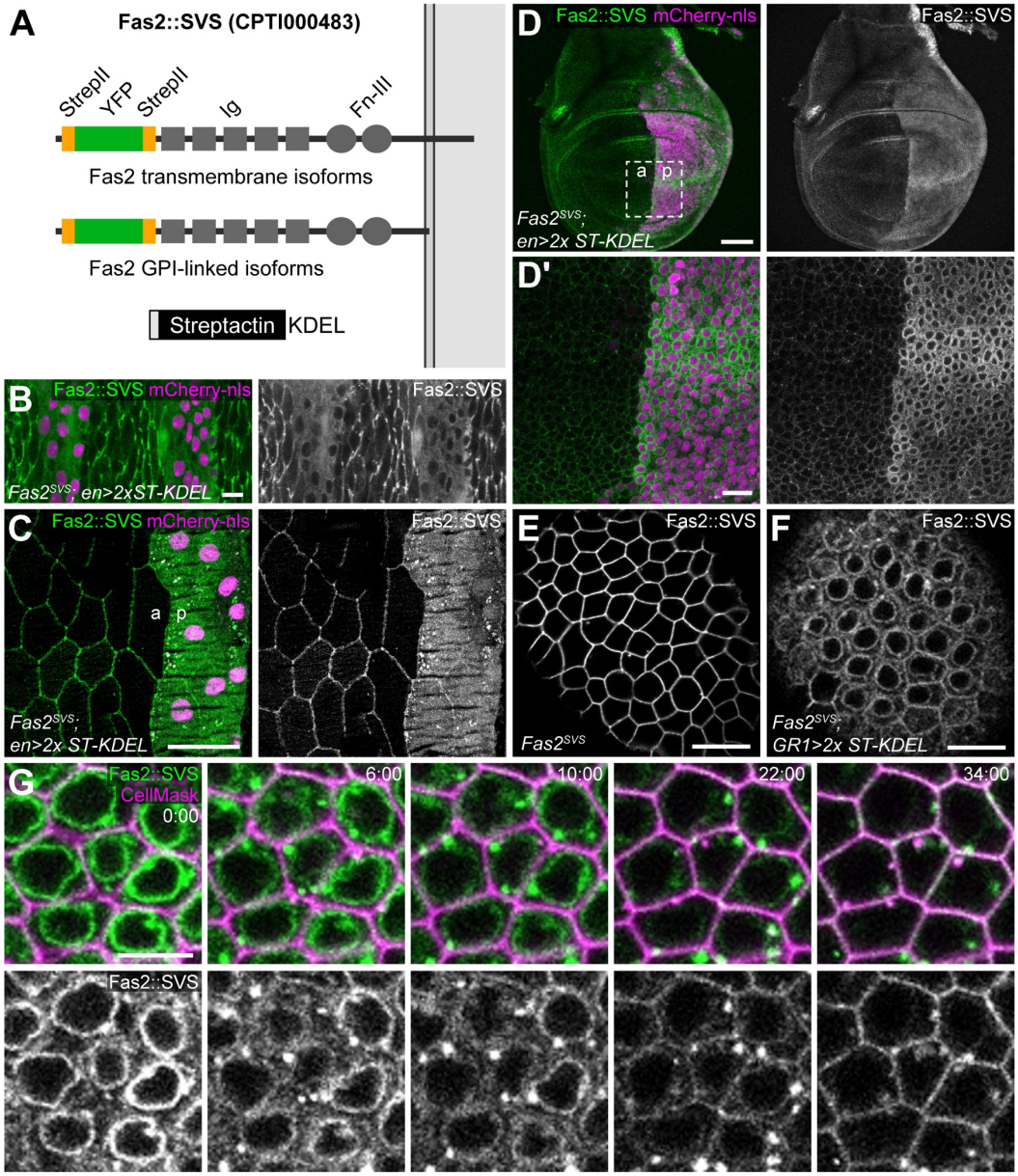
A
Fas2::SVS (CPTI000483)
StrepII
YFP
StrepII
Ig
Fn-III
Fas2 transmembrane isoforms
Fas2 GPI-linked isoforms
Streptactin
KDEL
B
Fas2::SVS mCherry-nls
Fas2SVS; en>2xST-KDEL
Fas2::SVS
C
Fas2::SVS mCherry-nls
a
p
Fas2SVS; en>2x ST-KDEL
Fas2::SVS
D
Fas2::SVS mCherry-nls
a
p
Fas2SVS; en>2x ST-KDEL
Fas2::SVS
D'
E
Fas2::SVS
Fas2SVS
F
Fas2::SVS
Fas2SVS; GR1>2x ST-KDEL
G
Fas2::SVS
CellMask
0:00
6:00
10:00
22:00
34:00
Fas2::SVS

958 **Figure 5**

959 **Manipulation of endogenous Fasciclin 2 protein *in vivo* and in cultured ovaries.**

960 **(A)** Scheme of Fasciclin 2 (Fas2) protein tagged with venus-YFP (green) flanked by StrepII
961 tags (orange). The *Fas2* locus encodes multiple transmembrane and GPI-linked isoforms, all
962 of which carry the extracellular StrepII-venus-YFP-StrepII (SVS) tag. For simplicity, only a
963 transmembrane isoform is shown. Streptactin-KDEL (bottom) mediates ER retention of
964 secretory proteins carrying StrepII tags in their luminal (extracellular) portion.

965 **(B,C)** Maximum-intensity projections of embryonic (B) and third instar-larval (C) epidermis
966 expressing Fas2::SVS (green). Two copies of Streptactin-KDEL and mCherry-nls (magenta)
967 are expressed in epidermal stripes under control of *en-Gal4*. Note that Fas2::SVS outlines
968 lateral membranes of control cells and accumulates in the ER of ST-KDEL-expressing
969 posterior (p) compartment cells marked by mCherry-nls.

970 **(D,D')** Maximum-intensity projection of wing imaginal disc of third-instar larva as in (B,C). Note
971 intracellular retention of Fas2::SVS in posterior (p) compartment. (D') shows close-up of region
972 marked by square in (D).

973 **(E,F)** Confocal section of follicular epithelium in cultured ovarian follicles (stage 7) from
974 *Fas2::SVS* females. Fas2::SVS localizes at lateral membranes in control egg chamber (E),
975 but is retained in the ER in Streptactin-KDEL-expressing follicle cells (F).

976 **(G)** Stills (confocal sections) from time-lapse movie of cultured egg chamber (stage 6)
977 expressing Fas2::SVS (green in G) and Streptactin-KDEL (two copies) in follicle cells.
978 CellMask (magenta) marks plasma membranes. After addition of biotin at t=0 min (1.5 mM
979 final concentration) to the medium, Fas2::SVS is released from the ER, accumulates in puncta
980 (6 min) and becomes detectable at the plasma membrane (22 min). Time (min:s) is indicated.
981 See Movie S8.

982 Scale bars: (B), 10 µm; (C,D), 50 µm; (D',E,F), 10 µm; (G), 5 µm.

# Figure 6

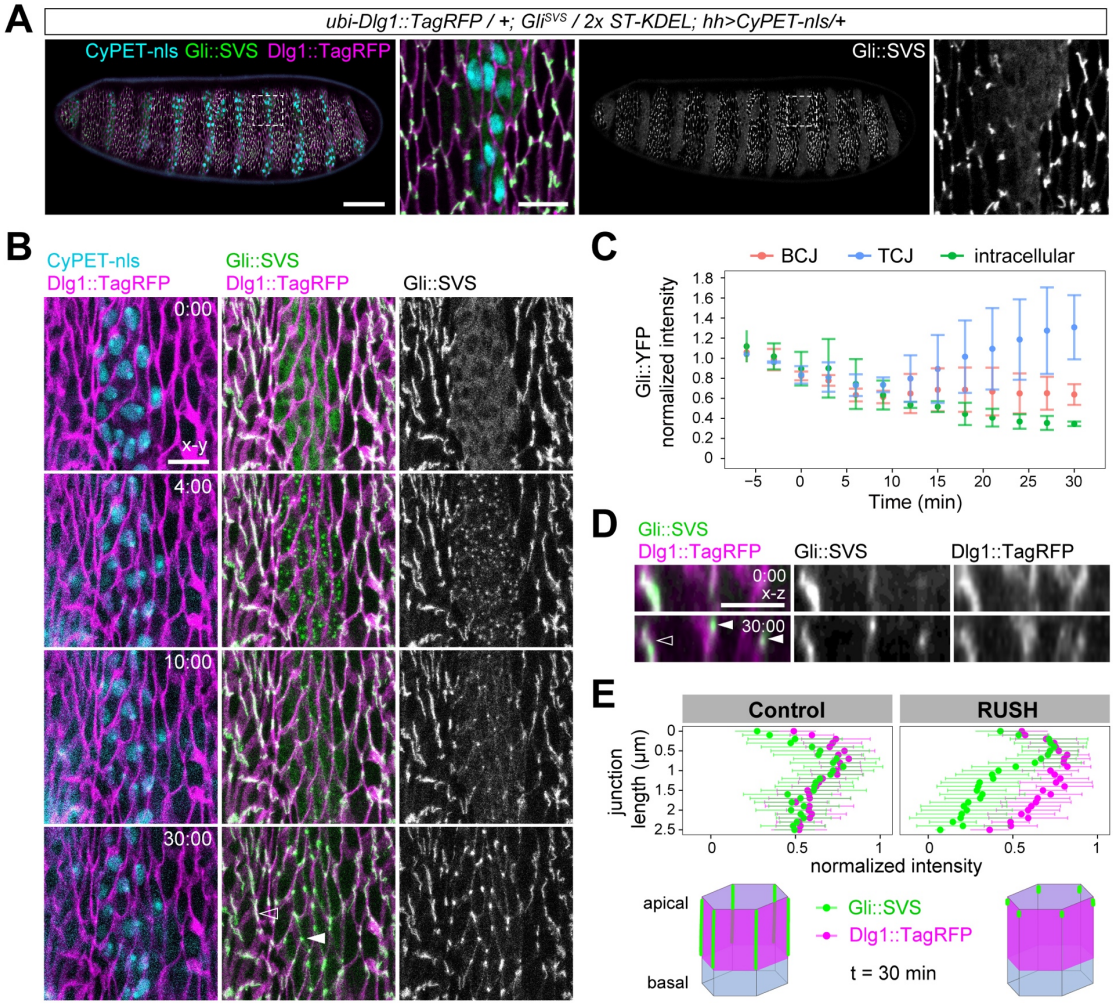
A
ubi-Dlg1::TagRFP / +; GliSVS / 2x ST-KDEL; hh>CyPET-nls/+
CyPET-nls Gli::SVS Dlg1::TagRFP
Gli::SVS
B
CyPET-nls
Dlg1::TagRFP
Gli::SVS
Dlg1::TagRFP
Gli::SVS
0:00
x-y
4:00
10:00
30:00
C
BCJ
TCJ
intracellular
Gli::YFP normalized intensity
Time (min)
D
Gli::SVS
Dlg1::TagRFP
Gli::SVS
Dlg1::TagRFP
0:00
x-z
30:00
E
Control
RUSH
junction length (µm)
normalized intensity
apical
basal
Gli::SVS
Dlg1::TagRFP
t = 30 min

984 **Figure 6**

985 **Real-time analysis of tricellular junction assembly in the embryonic epidermis.**

986 **(A)** Maximum-intensity projection of living embryo (stage 15) expressing endogenous Gli::SVS
987 (green) and *ubi*-Dlg1::Tag-RFP (magenta). CyPET-nls (cyan) and ST-KDEL (two copies) are
988 expressed in epidermal stripes under the control of *hh-Gal4*. Gli::SVS is retained in the ER of
989 CyPET-nls-marked ST-KDEL-expressing cells and accumulates along tricellular junctions in
990 control cells. Close-ups show region marked by box in overview panels.

991 **(B)** Stills (maximum-intensity projections) from time-lapse movie of embryo as in (A) injected
992 with biotin at t=0 min. After release from ER, Gli::SVS appears at ERES/Golgi puncta (t=4 min)
993 and subsequently begins to accumulate at tricellular junctions (t=10 min). White arrowhead
994 marks newly assembled Gli::SVS at apical tip of vertex in ST-KDEL expressing cell. Open
995 arrowhead marks extended Gli::SVS signal along vertex in control cell. Time (min:s) is
996 indicated. See Movie S7.

997 **(C)** Quantification of Gli::SVS signals at bicellular junctions (BJC, red), tricellular junctions
998 (TCJ, blue) and in the cytoplasm (green). Mean ± s.d. is shown. Per embryo and timepoint, 5
999 BCJs, 5 TCJs, and 5 cytoplasmic measurements were analyzed in a total of 3 embryos.

1000 **(D)** Sections acquired orthogonal (x-z) to the plane of the epithelium at the boundary of ST-
1001 KDEL-expressing cells and control cells. Note that newly released Gli::SVS is distributed along
1002 the apical-basal length of vertices in control cells (open arrowhead) but accumulates apically
1003 at vertices in ST-KDEL-expressing cells (white arrowheads).

1004 **(E)** Quantification of Gli::SVS (green) and Dlg1::Tag-RFP (magenta) signals (normalized to
1005 maximal signal) along TCJs in control cells (left graph) and ST-KDEL-expressing cells (RUSH;
1006 right graph) at t=30 min. TCJs extend from 0 µm (apical) to 2.5 µm (basal). Mean ± s.d. is
1007 shown. 5 junctions in control cells and 5 junctions in ST-KDEL-expressing cells per embryo
1008 were analyzed in 3 embryos.

1009 Scale bars: (A), 50 µm, close-ups: 10 µm; (B), 10 µm; (D), 5 µm.

Figure 7

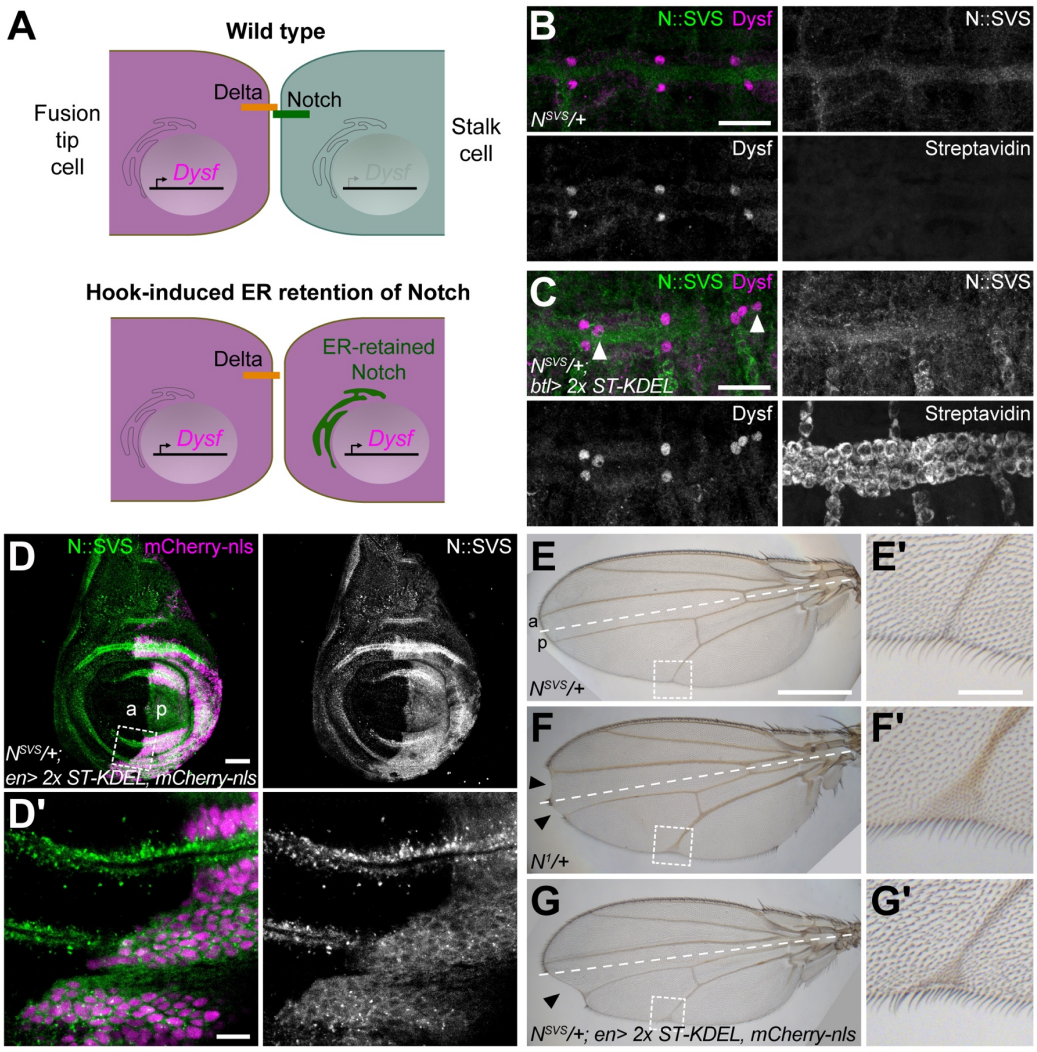
A
Wild type
Fusion tip cell
Delta
Notch
Stalk cell
Dysf
Hook-induced ER retention of Notch
ER-retained Notch
B
N::SVS Dysf
N::SVS
Dysf
Streptavidin
C
btl> 2x ST-KDEL
D
N::SVS mCherry-nls
en> 2x ST-KDEL, mCherry-nls
D'
E
E'
F
F'
G
G'
en> 2x ST-KDEL, mCherry-nls

1011 **Figure 7**

1012 **ER retention of Notch::SVS protein causes cell fate specification defects resembling**
1013 ***Notch* loss-of-function mutant.**

1014 **(A)** Role of Notch signaling in tracheal tip cell specification. The Notch ligand Delta on "fusion"
1015 tip cell (magenta) stimulates Notch signaling in adjacent stalk cell (green), preventing it from
1016 adopting tip cell fate. ER retention of Notch abolishes Notch signaling and leads to
1017 misspecification of stalk cells into tip cells.

1018 **(B,C)** Representative images of stage 15 *N::SVS/*+ control embryo (B) and *N::SVS/*+ embryo
1019 expressing ST-KDEL (two copies) in tracheal cells (C) stained with anti-GFP (to detect
1020 N::SVS; green), anti-Dysfusion (Dysf; magenta) and anti-streptavidin antibodies. Note weak
1021 N::SVS signals and a pair of Dysf-positive fusion cells at each tracheal metamere boundary
1022 in control embryo (B), whereas *btl*>ST-KDEL-expressing embryo shows intracellular retention
1023 of N::SVS and supernumerary Dysf-positive fusion cell nuclei (arrowheads in C).

1024 **(D,D')** Live wing imaginal disc of *N::SVS/*+ third-instar larva expressing ST-KDEL (two copies)
1025 and mCherry-nls in posterior compartment under control of *en-Gal4*. Note retention of N::SVS
1026 in the ER of posterior compartment cells marked by mCherry-nls. (D') shows close-up of boxed
1027 region at compartment boundary in (D).

1028 **(E-G')** Wings of control (*N::SVS/*+; E), $N^1$/+ (F), and *N::SVS/*+ flies expressing ST-KDEL (two
1029 copies) under control of *en-Gal4* (G). Note that ER-retention of N::SVS in the posterior
1030 compartment leads to wing margin notches (arrowheads in F,G) and enlarged wing veins
1031 resembling the phenotype of $N^1$/+ mutant but restricted to the posterior wing compartment.
1032 Close-ups (E',F',G') show enlarged view of distal L5 vein (boxed regions in E-G). Anterior (a)
1033 and posterior (p) compartments and the compartment boundary (dashed line) are indicated.
1034 Anterior is up.

1035 Scale bars: (B,C), 20 µm; (D), 50 µm; (D'), 10 µm; (E,F,G), 500 µm; (E',F',G'), 100 µm.